Early Life Neuroimaging: The Generalizability of Cortical Area Parcellations Across Development

Authors:
Jiaxin Cindy Tu[1], Michael Myers[2], Wei Li[3], Jiaqi Li[3,4], Xintian Wang[1], Donna Dierker[1], Trevor K. M. Day[5,6,7], Abraham Z. Snyder[1], Aidan Latham[8], Jeanette K. Kenley[8], Chloe M. Sobolewski[1,9], Yu Wang[3], Alyssa K. Labonte[2], Eric Feczko[5], Omid Kardan[10], Lucille A. Moore[5], Chad M. Sylvester[2], Damien A. Fair[5,6], Jed T. Elison[5,6], Barbara B. Warner[11], Deanna M. Barch[12], Cynthia E. Rogers[2], Joan L. Luby[2], Christopher D. Smyser[1,2,8,11], Evan M. Gordon[1], Timothy O. Laumann[1], Adam T. Eggebrecht[1], Muriah D. Wheelock[1]

Affiliations:
[1]Department of Radiology, Washington University in St. Louis.
[2]Department of Psychiatry, Washington University in St. Louis.
[3]Department of Mathematics and Statistics, Washington University in St. Louis.
[4]Department of Statistics, University of Chicago.
[5]Masonic Institute for the Developing Brain, University of Minnesota.
[6]Institute of Child Development, University of Minnesota.
[7]Center for Brain Plasticity and Recovery, Georgetown University.
[8]Department of Neurology, Washington University in St. Louis.
[9]Department of Psychology, Virginia Commonwealth University.
[10]Department of Psychiatry, University of Michigan.
[11]Department of Pediatrics, Washington University in St. Louis.
[12]Department of Psychological and Brain Sciences, Washington University in St Louis.

Corresponding Author
Muriah Wheelock
Mallinckrodt Institute of Radiology
4525 Scott Ave
St. Louis, MO 63110
mdwheelock@wustl.edu

Abstract

The cerebral cortex comprises discrete cortical areas that form during development. Accurate area parcellation in neuroimaging studies enhances statistical power and comparability across studies. The formation of cortical areas is influenced by intrinsic embryonic patterning as well as extrinsic inputs, particularly through postnatal exposure. Given the substantial changes in brain volume, microstructure, and functional connectivity during the first years of life, we hypothesized that cortical areas in 1-to-3-year-olds would exhibit major differences from those in neonates and progressively resemble adults as development progresses.

Here, we parcellated the cerebral cortex into putative areas using local functional connectivity gradients in 92 toddlers at 2 years old. We demonstrated high reproducibility of these cortical regions across 1-to-3-year-olds in two independent datasets. The area boundaries in 1-to-3-year-olds were more similar to adults than neonates. While the age-specific group parcellation fitted better to the underlying functional connectivity in individuals during the first 3 years, adult area parcellations might still have some utility in developmental studies, especially in children older than 6 years. Additionally, we provided connectivity-based community assignments of the

parcels, showing fragmented anterior and posterior components based on the strongest connectivity, yet alignment with adult systems when weaker connectivity was included.

Keywords

fMRI, functional connectivity, area, parcellation, development, lifespan

Introduction

Understanding the intricate organization of the human brain is a fundamental pursuit in systems neuroscience. Previous research has supported the notion that the cerebral cortex is divided into spatially contiguous areas distinguishable by function, architecture, connectivity, and/or topographic organization (Felleman and Van Essen, 1991; Glasser *et al.*, 2016; Petersen *et al.*, 2024). It has been hypothesized that the patterning of cortical areas starts during embryonic development to form a "protomap" organization (Fukuchi-Shimogori and Grove, 2001), while extrinsic factors refine this "protomap" into discrete areas (O'Leary, Chou and Sahara, 2007; Cadwell *et al.*, 2019). One important extrinsic factor in this process is the input to the cortex from thalamocortical axon projections (O'Leary, Chou and Sahara, 2007), which undergo refinements driven by sensory inputs (Catalano and Shatz, 1998; Tau and Peterson, 2010; Smyser, Snyder and Neil, 2011). The explosive increase in exposure to environmental stimuli following birth likely plays a significant role in the refinement of area boundaries shortly after birth. Moreover, synaptic addition and growth of dendrites and spines also enters a phase of logarithmic growth in the first few months after birth (Levitt, 2003), suggestive of an elevated period of cortical plasticity. Considering these factors, it is reasonable to expect that cortical areas in neonates would show low similarity to those in adults (Myers *et al.*, 2024), with greater similarity between infant and adult brain areas as the brain develops. Furthermore, it has been postulated that developmental changes are not uniform across the brain. The sequence of development has previously been described to follow a sensorimotor-to-association axis (Flechsig, 1901; Casey *et al.*, 2005; Hill *et al.*, 2010; Tau and Peterson, 2010; Smyser and Neil, 2015; Smyser *et al.*, 2016; Grayson and Fair, 2017; Sydnor *et al.*, 2021), or a posterior-to-anterior axis (Larivière *et al.*, 2020; Q. Li *et al.*, 2024). Few studies have examined whether the maturation of cortical areas followed either of these patterns.

Many neuroimaging analyses have been conducted at the scale of parcels (Zalesky *et al.*, 2010; Arslan *et al.*, 2018; Farahani, Karwowski and Lighthall, 2019; Bijsterbosch *et al.*, 2020; Faskowitz, Betzel and Sporns, 2022, 2022; Helwegen, Libedinsky and Heuvel, 2023; Luppi *et al.*, 2024). Inaccurate parcellation choice can lead to the mixing of signals (Smith *et al.*, 2011), conceal known community structure (Power *et al.*, 2011), and reduce the prediction accuracy of clinical phenotypes (Abraham *et al.*, 2017). Therefore, choosing a parcellation scheme that closely reflects the actual area boundaries in the data is of great importance for functional connectivity (FC) analyses (Grayson and Fair, 2017).

Neuroimaging analyses often adopt definitions of cortical areas in adult brains (Shen *et al.*, 2013; Glasser *et al.*, 2016; Gordon *et al.*, 2016; Schaefer *et al.*, 2018). However, the dynamic and rapid development of the brain during infancy (Bethlehem *et al.*, 2022) triggers unique concerns about whether it is valid to apply existing adult area parcellations to infant brains (Cusack, McCuaig and Linke, 2018; Shi *et al.*, 2018; Oishi, Chang and Huang, 2019; Wang *et al.*, 2023). In response, several

infant-specific area parcellations have been developed in recent years (Scheinost *et al.*, 2016; Shi *et al.*, 2018; Wang *et al.*, 2023; Myers *et al.*, 2024). Despite these advances, having different area parcellations for different age ranges poses a practical challenge for making coherent comparisons in brain organization across development. Thus, many researchers have continued to use adult parcellations in infant studies (Nielsen *et al.*, 2022; Kim *et al.*, 2023; Yates, Ellis and Turk-Browne, 2023), as well as studies across the lifespan (Betzel *et al.*, 2014; Cao *et al.*, 2014; Zuo *et al.*, 2017; Puxeddu *et al.*, 2020).

One crucial factor in determining which parcellation to employ in a given age range would be the degree to which an age-specific parcellation differs from an adult parcellation in pediatric samples. However, a systematic examination of parcellations across age groups is lacking. We aim to a) illustrate how well the area parcellations fit the functional connectivity data across individual infants/children at various developmental stages, b) quantify the improvement compared to adult parcellations, and c) evaluate the potential impact of of using an adult parcellation instead of the proper infant parcellation on downstream analyses. If adult parcellations separate the cortical areas with comparable success as infant parcellations, utilizing adult parcellation schemes for developmental cohorts would be justifiable. One prior study suggested that this was not the case for neonates (Myers *et al.*, 2024). Here we query whether the adult parcellation would be a reasonable choice for older infants, toddlers and children.

In the current study, we derived a surface-based area parcellation based on FC local gradient transitions (Cohen *et al.*, 2008; Wig, Laumann and Petersen, 2014; Gordon *et al.*, 2016) in 92 toddlers at age of 2 years. To test the reproducibility of our area parcels across groups of subjects and whether the reproducibility followed a uniform distribution across space, we derived parcellations using half the sample (n = 46). To examine differences in patterns of FC local gradient transition across development, we quantified the similarity between the boundary maps at different developmental stages. Furthermore, we compared our area parcellation to alternative adult and infant parcellations and demonstrated the generalizability and limitations of our area parcellation for application to various developmental stages. Finally, we derived the community organization which described the relationship between the area parcels.

Methods

Neuroimaging Data of Infants/Toddlers for Deriving Area Parcellations

One main goal of this paper is to examine the area parcellations at age 1-3. We used two infant/toddler datasets: eLABE (Y2) and BCP (Table 1). The infant/toddler datasets used in the current study were all collected with a Siemens Prisma 3T scanner using HCP-style acquisition parameters (Supplementary Table 1). The functional MRI acquisition lasts 420 frames per scan run with 2-4 runs in Baby Connectome Project (BCP) and 1-8 runs in the Early Life Adversity, Biological Embedding (eLABE) 2-year-old data (Y2). Anatomical scan processing and segmentation were conducted using age-specific pipelines (Kaplan *et al.*, 2022). Functional data preprocessing largely followed established procedures (Power *et al.*, 2014). Toddler EPI BOLD preprocessing pipeline was used for eLABE (Y2) and DCAN-Infant v0.0.9 (Glasser *et al.*, 2013; Donahue *et al.*, 2016; Autio *et al.*, 2020) were used for BCP. Motion correction was performed with rigid-body transforms. Additionally, the functional data were corrected for asynchronous slice time shifts and

systematic odd-even slice intensity differences attributable to interleaved acquisition (Power *et al.*, 2012). The data were intensity normalized to achieve a consistent whole-brain mode value, and subsequently resampled to atlas space before being projected onto the 32k_fs_LR standard surface (Van Essen *et al.*, 2012). Denoising was accomplished by nuisance regression, with regressors consist of a 24-parameter Volterra expansion of motion time series, the mean signal over gray-ordinates, and the mean signals derived from white matter and cerebrospinal fluid (CSF) compartments. The data were bandpass filtered to retain BOLD-specific frequencies and geodesically smoothed with Connectome Workbench (Marcus *et al.*, 2011; Glasser *et al.*, 2013). Frame censoring was performed based on the frame displacement time series (FD > 0.2mm) following age-specific notch-filtering to exclude respiratory frequencies (Kaplan *et al.*, 2022). Structural and functional scans were manually inspected and runs/sessions that failed quality controls were discarded. Additionally, participants who were born preterm (<37 weeks gestational age), had any neonatal ICU experience, or had signs of injury on MRI were also excluded from the analysis. Functional data with less than 600 low-motion frames were also excluded. For additional dataset-specific details, see Supplementary Table 1.

A summary of the demographics and image quality of the developmental cohort discovery and validation datasets is provided in Table 1. The cross-sectional age distribution and the distribution of age in longitudinal sessions are displayed in Supplementary Figure 1.

Table 1. *Subject demographics for the two infant/toddler datasets.* For continuous variables, the mean is provided along with standard deviations in brackets. The group identity was defined as the median age rounded to the nearest whole number.

Group	Age (months)	Age Range (months)	Number of participants	Average retained FD (mm)	Frame retention rate (%)	Acquisition time	% White	% Male
eLABE (Y2)								
25 mo	25.2 (1.8)	22-31	92	0.068 (0.021)	92 (9)	20.0 (4.6)	21	59
BCP								
10 mo	9.70 (0.71)	8-10	30	0.080 (0.014)	80 (6)	16.4 (5.3)	70	50
12 mo	12.32 (0.80)	11-13	37	0.076 (0.017)	83 (6)	13.3 (4.7)	78	57
16 mo	15.47 (0.88)	14-16	39	0.079 (0.015)	80 (8)	17.6 (5.5)	79	38
19 mo	19.14 (1.52)	17-22	37	0.078 (0.017)	82 (8)	16.4 (5.8)	81	57
25 mo	25.38 (1.60)	23-28	34	0.078 (0.016)	83 (5)	16.7 (5.5)	74	53

Neuroimaging Data for Comparing FC Boundaries Across the Lifespan

To compare FC boundaries, we additionally included the FC boundaries from a young adult dataset (Washington University 120, WU120) used in a widely adopted adult parcellation (Gordon *et al.*, 2016) and from the same neonate dataset (eLABE

(Birth)) used in a neonatal parcellation (Myers *et al.*, 2024). Acquisition and processing of these datasets followed similar pipelines to the infant/toddler datasets above and as briefly described below. For dataset-specific details, please refer to Supplementary Table 2.

WU120

Data were collected from 120 healthy young adult participants recruited from the Washington University community during relaxed eyes-open fixation (50% male, ages 19–32). Scanning was conducted using a Siemens TRIO 3T scanner and included the collection of high-resolution T1-weighted and T2-weighted images, as well as an average of 14 min of resting-state fMRI. Detailed acquisition and processing have been reported previously (Power *et al.*, 2014).

eLABE (Birth)

Inclusion criteria were the same as the eLABE (Y2) cohort. Neuroimaging data were collected in 261 full-term, healthy neonate offspring shortly after birth (average postmenstrual age of included participants 41.7 weeks, range 39–45 weeks, 54% male). A total of 131 participants with the most data following frame censoring were used to create the FC boundaries. Additional details are in Supplementary Table 2.

Neuroimaging Data for Testing the Generalizability of Areas Across the Lifespan

To test for the generalizability of area parcellations across the lifespan, we additionally include the year-3 timepoint from the eLABE dataset, Healthy Brain Network (HBN) children dataset, and HCP young adult (HCP-YA) dataset.

eLABE (Birth)

This is the same dataset as above. Because 131 of the participants were involved in the creation of the Myers-Labonte parcellation (Myers *et al.*, 2024), the other 130 participants *not used in the parcel generation* were used to test the parcellation's cluster validity performance to prevent circularity. The acquisition protocol and processing pipeline were the same as described before (Supplementary Table 2).

eLABE (Y3)

The inclusion criteria were the same as the eLABE (Y2) cohort. Neuroimaging data were collected from 132 participants at the age of 3 years. Additional participants were excluded based on the quality of structural and functional data and having less than 8 min (600 frames) of low-motion (respiratory-filtered FD < 0.2) data retained, leaving 65 participants (range = 2.93-3.97 years, mean = 3.22 years, SD = 0.32 years, 63% male). The acquisition protocol and processing pipeline were the same as the eLABE (Y2) dataset at age two.

HBN

Resting-state fMRI data from 493 participants from the first nine releases of the Healthy Brain Network (HBN) were divided into 10 groups by year (6-15yr). The HBN study is a large, multi-site study of children and young adults ages 5–21 years all collected in the New York area. Recruitment, consent, and study procedures are described in the data publication (Alexander et al., 2017) as well as project website. We used the data from two sites (CitiGroup Cornell Brain Imaging Center (CBIC) and Rutgers University Brain Imaging Center (RUBIC)).

Data were pre-processed using the Human Connectome Project minimal processing pipeline (Glasser et al., 2013). Additional processing steps (demeaning, detrending, nuisance regression (with regressors consist of a 24-parameter Volterra expansion of motion time series, the mean signal over gray-ordinates), bandpass filtering at 0.008-0.1 Hz to retain BOLD-relevant frequency and frame censoring at FD > 0.2 mm threshold) were carried out using custom-written Python (v3.8) scripts using the numpy v1.24.4, scipy v1.10.1, nibabel v5.1.0, and pandas v2.0.3 libraries. Each scan session takes 10 min and all included sessions comprises at least 8 min (600 frames) of low-motion (respiratory-filtered FD < 0.2) data retained. Data was geodesically smoothed to achieve an effective smoothing of 2.55 sigma gaussian kernel.

HCP-YA

Resting-state fMRI data from a subset of randomly chosen 40 participants not used for the creation of the Glasser parcellation (Glasser *et al.*, 2016) were selected from the HCP-YA dataset for external validation of the adult dataset to minimize circularity. Data was processed with the same standard preprocessing pipeline as WU 120, except that a respiratory-filtered FD < 0.04 mm was used to remove high-motion frames.

Creation of FC-transition Boundary Maps and Area Parcels

We segmented the cortical surface into discrete parcels representing putative cortical areas based on the FC local gradient (Gordon *et al.*, 2016). The FC from each vertex to every other vertex was calculated as Pearson's correlation of the time series in individual sessions (Supplementary Figure 2A). The Fisher-Z-transformed FC from each vertex was correlated with a randomly subsampled set of 594 vertices (1% of the total vertices) to generate an "FC similarity" matrix, which indexed the similarity in FC patterns across vertices (Supplementary Figure 2B). We used 1% of the vertices for computational efficiency without compromising accuracy (Supplementary Materials). After that, the workbench command "cifti-gradient" was used to calculate the gradient of FC-transition in individual subjects' surfaces in the standard 32k_fs_LR mesh. The gradient maps were then averaged across all subjects and smoothed with a Gaussian kernel of 2.55 sigma (Supplementary Figure 2C). A "watershed by flooding" algorithm (Beucher and Meyer, 1992) was used to create discrete areas separated by boundaries based on the gradient transitions (Supplementary Figure 2D). The gradient-based boundary map technique rests on the assumption that FC within a cortical area is relatively uniform and distinct from FC of an adjacent area (Wig, Laumann and Petersen, 2014), similar to how areas were distinct in connectivity in macaque monkeys (Felleman and Van Essen, 1991). Finally, the boundaries from different gradient maps were averaged to obtain a boundary map that indexed the probability of a vertex being an area boundary (value ranges between 0 and 1) (Supplementary Figure 2E).

Discrete parcels (Supplementary Figure 2F) from a boundary map were created by locating the minima in the boundary map, growing parcels from minima using the watershed algorithm, and merging the watersheds if the median values of boundaries between them are below a threshold (merging threshold, defined as a percentile of the boundary map values). Neighboring parcels with sizes smaller than 15 vertices were merged. Parcels joined only by a single vertex were split. Isolated parcels smaller than 10 vertices were removed. Vertices above 90% in the boundary map values (height threshold) were left as parcel borders. The resolution of the parcels depends on the

merging threshold, with higher merging thresholds leading to a small number of larger parcels and lower merging thresholds leading to a large number of smaller parcels. We varied the merging threshold from 20% to 90% (Supplementary Figure 3).

Parcel Reproducibility

To assess the reproducibility of our results, we generated the boundary map (Supplementary Figure 2E) and discrete parcels (Supplementary Figure 2F) from non-overlapping split halves of participants 20 times. For each pair of parcellations at a merging threshold, we quantified the overlap in the parcels and in the boundaries (See Section: **Parcel Similarity Measures**). In addition, we divided the brain into 10 equal bins based on either the position along the sensorimotor-association axis (Sydnor *et al.*, 2021) or the posterior-anterior axis and calculated the parcel reproducibility in each bin (Supplementary Figure 4).

Parcel Similarity Measures

Adjusted Rand Index (ARI) calculated on non-boundary vertices was used as the main measure of similarity across two parcellations. For completeness and comparability with prior literature, we also calculated the dice coefficient between parcellations, either as the average dice coefficient across matching pairs of parcels defined with the largest dice coefficient (Shen *et al.*, 2013), or on binarized parcel identity maps (with boundaries as 0 and parcels as 1) (Myers *et al.*, 2024). The dice coefficient between binarized parcel identity maps was biased by the percentage of the brain covered with parcels (e.g. when there are more/wider boundaries, the overlap will be higher). For example, in parcellations such as Glasser (Glasser *et al.*, 2013) and AAL (Tzourio-Mazoyer *et al.*, 2002), the dice coefficient calculated this way would be 1 because those parcellations did not specify boundaries and allocate all cortical vertices into parcels.

Additionally, we compared the binarized parcel boundaries (with boundaries as 1 and parcels as 0). We quantified the differences between the parcel boundaries with dice coefficient and Hausdorff distance (Shen *et al.*, 2013; Müller, Soto-Rey and Kramer, 2022), which measures the maximum distance one needs to travel between two contours. A lower Hausdorff distance indexed a high similarity between boundaries. We used a spatial distance measure for boundaries because it is less sensitive to small shifts in space and does not require perfect overlap. To mitigate sensitivity to, we used two variants of the Hausdorff distance measure: 95% Hausdorff distance (HD95) (Huttenlocher, Klanderman and Rucklidge, 1993) and average Hausdorff distance (AHD) (Müller, Soto-Rey and Kramer, 2022). HD95 was defined as the maximum of the 95th percentile of the distances between any point in contour X to the closest point in another contour Y and the 95th percentile of the distances between contour Y to the closest point in contour X. AHD was defined as the maximum of the mean distance between contour X and contour Y and the mean distance between contour Y and contour X.

$$HD95 = \max\big(d95(X,Y), d95(Y,X)\big) \ [Equation\ 1]$$

$$AHD = \max\Big(\bar{d}(X,Y), \bar{d}(X,Y)\Big) \ [Equation\ 2]$$

Here “distance” was defined as the geodesic distance between vertices in the Conte69 surface atlas (Van Essen *et al.*, 2012).

Additionally, we generated a null model by generating random rotations around the x,y, and z axes for a split-half of the total sample of data (Split-I) and calculated each of the metrics. In theory, this controls for the bias from different merging thresholds, but due to the presence of the medial wall, spatial permutations often induce missing data (Markello and Misic, 2021).

Boundary Map Consistency Across Age

To examine the difference in the area organization across different developmental stages, we applied the same method to generate boundary maps from neonates and adults. These were compared to the boundary maps derived from the eLABE (Y2) dataset. We computed the similarity between the boundary maps by taking the top percentiles of the boundary map values and calculating the Hausdorff distance measures.

Evaluation of Cluster Validity of Area Parcellation

To evaluate the cluster validity of the area parcellations (i.e. how well they fit the FC data, we used an unbiased metric for the comparison of parcellations across different spatial resolutions (Zhi *et al.*, 2022). The distance-dependent boundary coefficient (DCBC) (Zhi *et al.*, 2022) compares the average difference in similarity (Pearson's r, with a value between -1 and 1) of FC profiles from vertices within a parcel and those from vertices between parcels across geodesic distance bins of 1 mm (e.g. between 10 mm to 11 mm). As demonstrated in a prior publication (Zhi *et al.*, 2022), this metric accounts for the spatial smoothness of the data and is relatively unbiased when comparing parcellations across multiple spatial resolutions (a.k.a. number of parcels). The expected value of DCBC for a random parcellation was zero regardless of the resolution of the parcellation, and a positive DCBC would mean better than random. Thus, no simulation with random null parcellations is necessary to establish a baseline measurement, as opposed to measures like homogeneity Z-score compared to a spatially permuted null (Gordon *et al.*, 2016). As a negative control, we also evaluated a parcellation that randomly partitioned the brain into 304 equally-sized fragments (Icosahedron) as a control. For implementation details and a comparison with alternative measures, please refer to the Supplementary Materials.

Comparing Our Area Parcellation to Alternatives

To further contextualize results, we compared our area parcellation to existing area parcellations created using adult or infant data. We transformed the area parcellations into the common 32k_fs_LR standard mesh where necessary. Details for the transformation are provided in the Supplementary Materials.

Table 2 summarizes the parcellations tested including the number of parcels, sources, and original space. In addition, to establish a lower bound of DCBC for the dataset, we used an Icosahedron-162 parcellation which provided regular tessellations of the hemispheres in the form of a 3D regular polyhedron with equilateral triangles as faces (Zhi *et al.*, 2022).

Table 2. *Adult and Infant Area Parcellations*

Name	Number of parcels	Citation	Original Space
Gordon	333	Gordon, Laumann et al. 2016	32k_fs_LR

Glasser	360	Glasser et al. 2016	32k_fs_LR
Schaefer	400	Schaefer et al. 2018	32k_fs_LR
AAL	82	Tzourio-Mazoyer et al. 2002	MNI152
Desikan	70	Desikan et al. 20016	32k_fs_LR
Shen	200	Shen et al., 2013	MNI152
Myers-Labonte	283	Myers, Labonte et al., 2024	32k_fs_LR
Tu	326	Current study	32k_fs_LR
Wang	864	Wang et al. 2023	32k_fs_LR
Scheinost	87	Scheinost et al., 2016	MNI152
Shi 1 Yr	194	Shi et al., 2018	Age-specific T1 (Shi et al., 2011)
Shi 2 Yr	205	Shi et al., 2018	Age-specific T1 (Shi et al., 2011)
Icosahedron (control)	304	Zhi et al. 2022	32k_fs_LR

Comparing Our Area Parcellation to Age-specific Infant Area parcellations

Using the boundary maps in Figure 2, we generated age-specific area parcellations with the BCP data divided into 5 groups and a merging threshold of 65%. To test whether finer age-specific parcellation improves cluster validity in infants/toddlers at a certain age, we calculated the DCBC for these five age-group parcellations on a secondary validation dataset containing an additional subset of BCP sessions in the same age range (N = 73 sessions from 51 participants, age range 8-29 months). This validation datset included more recently released BCP data collected at the University of Minnesota and University of North Carolina Chapel Hill sites. Acquisition and processing details were largely the same as the main BCP dataset described before with an update to the DCAN-Infant pipeline v0.0.22 where zero-padding has been implemented at the filtering step to minimize the distortions in the edges of the time series.

Practical Implications of Using Infant and Adult Parcellations

Previously, researchers have found that inaccurate parcellation may reduce the prediction accuracy of clinical phenotypes (Abraham *et al.*, 2017; Dadi *et al.*, 2019).

FC derived from an accurate parcellation should yield satisfactory prediction accuracies for behavioral phenotypes (Kong *et al.*, 2023) and demonstrate decent test-retest reliability (Tozzi *et al.*, 2020). We thus compare the prediction accuracy of age using FC from BCP dataset based on the present 2-year-old parcellation (Tu (326)) and the Gordon parcellation (Gordon *et al.*, 2016), which were the best-performing infant and adult parcellations on cluster validity respectively. In addition, we assessed the test-retest reliability of individual edges in the parcellated FC. We constructed a functional connectome with the first 7.2 min (600 frames for TR = 0.8 and 540 frames for TR = 0.72) of low-motion (filtered FD<0.2) fMRI data in each subject in the BCP dataset using the parcellations and applied a linear support vector regression for the prediction of age (J. Li *et al.*, 2024). The test-retest reliability was assessed with the first 5 min of two separate scan runs within the same session using an intraclass correlation coefficient (ICC (3,1))(Shrout and Fleiss, 1979; Tozzi *et al.*, 2020). Details are provided in the Supplementary Materials.

Identification of Community Structure in 2-year-olds

To characterize the relationship between the area parcels, we identified the community structure with the Infomap algorithm on the area parcels as nodes and the FC between parcels as edges (Rosvall and Bergstrom, 2008; Gordon *et al.*, 2016). For each participant in the eLABE (Y2) dataset (N = 92), we created a parcellated time series by calculating the mean within-parcel time series over each of the parcels from the dense grayordinate time series in 32k_fs_LR space with the workbench command "wb_command cifti-parcellate". We then cross-correlated these parcellated time series to generate a parcel-wise correlation matrix. Parcel-wise correlation matrices were Fisher z-transformed and averaged across all participants to obtain a group-average correlation matrix.

To reduce the impact of non-neuronal sources of inflation in short-distance correlation (e.g., data processing, subject motion), we applied an exclusion distance of 30 mm on the correlation matrix. A range of thresholds was then used to make the parcel-wise correlation matrix into a weighted sparse graph (edge density in steps of 0.25% ranging from 0.25% to 20%), which were entered as inputs to the Infomap algorithm. A consensus across thresholds was found with a manual examination of the communities at different thresholds to identify reliable networks across thresholds which also matched the prior description of functional systems (Power *et al.*, 2011; Yeo *et al.*, 2011; Wig, 2017). In addition, we also examined whether the networks at lower edge density thresholds, keeping the naming convention and colors similar to what was described in an earlier publication (Myers *et al.*, 2024).

Results

Area Parcellation in 2-year-olds is Reproducible across Participants

The reproducibility of the area parcellations across participants was evaluated using split-half sampling 20 times (Figure 1A-B). We found that the reproducibility was highest around a merging threshold of 60-80%, significantly larger than the spatially permuted null model (Figure 1C-E). Based on manual inspection of the boundary map and the granularity of area parcels in popular adult area parcellations (Glasser *et al.*, 2016; Gordon *et al.*, 2016), we settled on a merging threshold of 65% for our main parcellation, which produced 324-391 parcels across 20 split-haves (Supplementary Figure 5A). For the remaining sections, the main area parcellation using all data in eLABE (Y2) (N = 92) and merging threshold 65% were used for evaluation, hereafter

referred to as “Tu (326)”. At the merging threshold of 65%, ARI = 0.66 $\pm$ 0.02, Z-score compared to the null model = 14.3, parcel averaged dice coefficient = 0.62 $\pm$ 0.01, Z-score compared to the null model = 15.2. The dice coefficient for the binarized parcel map is 0.87 $\pm$ 0.002, Z-score compared to the null model = 8.46. Similar results were obtained with binarized boundary maps (see Supplementary Materials).

Furthermore, we examined the parcel reproducibility across different positions in the brain by segmenting the brain into approximately 10 equal divisions along the sensorimotor-association axis (Supplementary Figure 4A) and the posterior-anterior axis (Supplementary Figure 4B). We found that the sensorimotor regions tend to have higher reproducibility than the association regions (Figure 1F-H) and that the posterior regions tend to have higher parcel reproducibility than the anterior regions (Figure 1I-K).

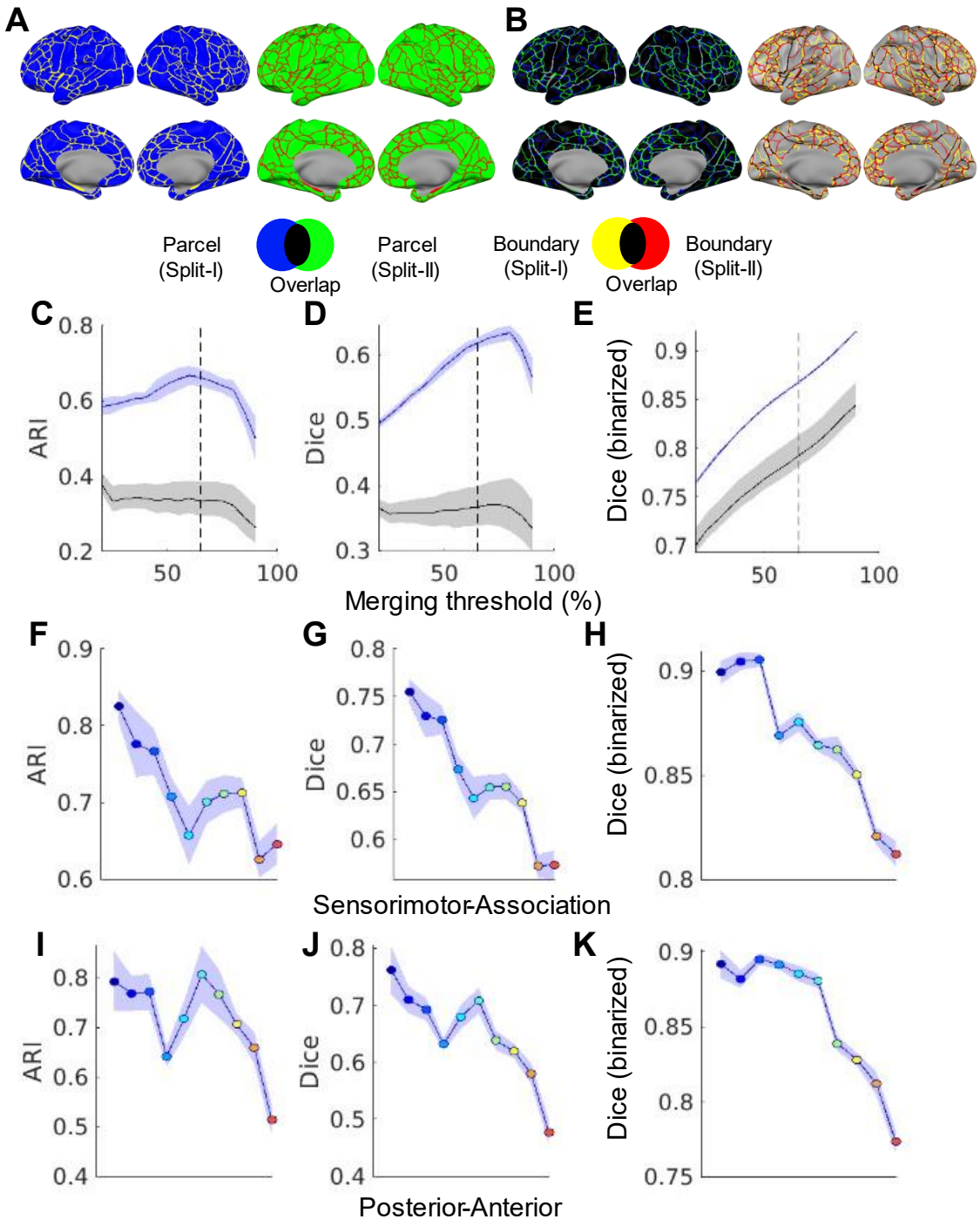

Figure 1. *Parcel reproducibility between split halves.* A) Parcellations from an example first split-half and and second split-half. B) The overlap between the parcels and boundaries in A and B. C) Adjusted Rand Index (ARI). D) parcel-average Dice coefficient. E) Dice coefficient on binarized parcels. The blue line and shaded area show the actual values and the standard deviation across 20 splits. The black line and shaded area illustrate the mean and 95% confidence interval of the spatially permuted null from one example split. The dashed line shows the merging threshold = 65%. F-H: the same metrics in C-E but separated into 10 bins along the Sensorimotor-Association axis at merging threshold = 65%. I-K: the same metrics in C-E but separated into 10 bins along

Boundary Maps in 2-year-olds Resembled Adult Boundary Maps More than Neonate Boundary Maps

We compared the boundary maps from the 2-year-olds (Figure 2A-B) to boundary maps generated from adults (Figure 2C) and neonates (<1 month from birth, Figure 2D) by comparing the similarity of the vertices with the top percentile of boundary probabilities (ranging from 15-55%) (Supplementary Figure 6).

Boundaries in 2-year-olds were spatially closer to adult boundaries (HD95 = 7.61 ± 0.24 mm, AHD = 2.22 ± 0.03 mm for the top 35% vertices) compared to neonate boundaries (HD95 = 8.68 ± 0.01 mm, AHD = 2.63 ± 0.01 mm for the top 35% vertices) (Figure 2E-F).

The boundaries were considerably similar across the five infant/toddler age bins (median age 10, 12, 16, 19, 25 months, Table 1) in the BCP dataset (HD95 $\approx$ 5 mm for the top 35% vertices, Supplementary Figure 7). However, area boundaries tended to be more similar between infant/toddler groups with a smaller age difference.

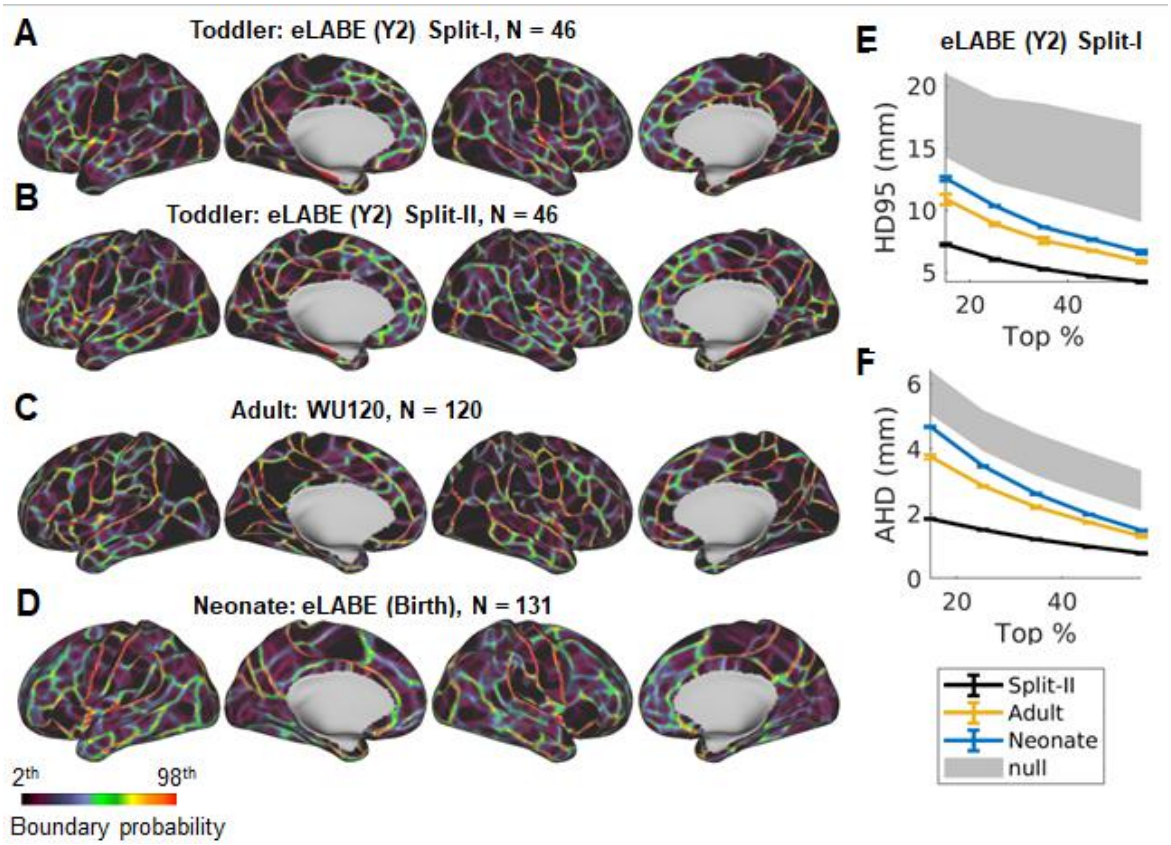

Figure 2. *Similarity of boundary maps across ages*. A) The FC boundary map in an example first split half. B) The FC boundary map in an example second split half. C) The FC boundary map in an adult dataset (WU 120). D) The FC boundary map in a neonate dataset (eLABE (Birth)). (E) 95% Hausdorff distance (HD95) indexes the spatial similarity of the boundaries between eLABE (Y2) Split-I and those from eLABE (Y2) Split-II (black), adult (yellow), and neonate (blue). The shaded area indexes the 95% confidence interval for the HD95 between the FC boundary in eLABE (Y2) Split-I and 1000 spatially permuted null of eLABE (Y2) Split-II. F) Same as E but using average Hausdorff distance (AHD). Lower HD95 and AHD indicate more similar boundaries.

Local Gradient-Based 2-year-old Area Parcellation Provides the Best Cluster Validity for infants and toddlers at 8-31 months

Using FC profiles from the eLABE (Y2) individuals, we evaluated the cluster validity of the present 2-year-old parcellation versus several extant adult and infant

area parcellations (Figure 3A), as well as the Icosahedron parcellation with 304 parcels (Supplementary Figure 8) using FC from eLABE (Y2) individuals. We observed a large variation in cluster validity within adult and infant parcellation groups, with the Gordon parcellation demonstrating the best performance among adult parcellations and the Tu (326) parcellation demonstrating the best performance among infant parcellations (Figure 3B). However, all adult and infant parcellations examined except for AAL (82) and Desikan (70) had DCBC > 0 (FDR-corrected $p<.05$). The DCBC for the control Icosahedron (304) parcellation was not significantly above 0. A repeated measures ANOVA with the 13 parcellations as the within-subject factor was run on the 13x92 DCBC matrix and demonstrated a significant difference in DCBC across parcellations, $F(12,1092) = 508.64$, $p<.001$). Post-hoc paired t-test showed that Tu (326) had a better cluster validity (Cohen's $d > 2.0$, Supplementary Figure 9A)

than alternative adult and infant parcellations in eLABE (Y2) individuals.

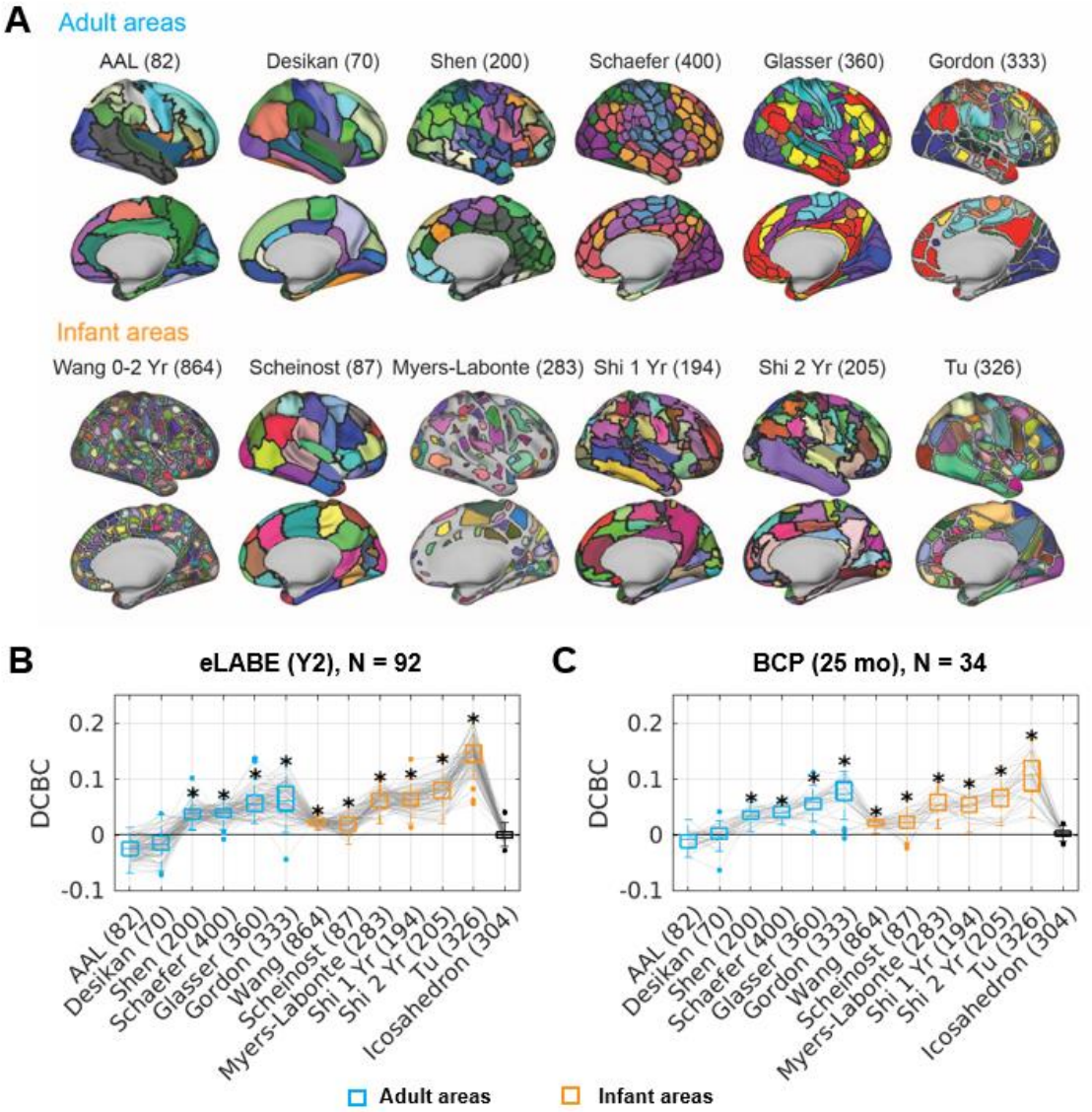

Figure 3. *Cluster validity for different area parcellations evaluated with a distance-controlled boundary coefficient (DCBC) measure.* (A) Adult area parcellations and infant area parcellations. (B) DCBC quantified in individuals in the same eLABE (Y2) dataset used to derive the Tu (326) parcels. (C) DCBC quantified in individuals in an independent dataset (BCP). * p<.05 after FDR correction for one-sample t-test against 0. As a convention, we noted the number of parcels of a particular parcellation scheme in parentheses, e.g., Gordon (333) means Gordon parcellation with 333 parcels

One caveat to the observation above was that the evaluation was performed on the same dataset used to generate the parcels. As such, an independent validation dataset (BCP) was used to further evaluate the cluster validity of the area parcellations (Figure 3C). The Gordon (333) and Tu (326) parcellations still performed the best within their respective parcellation age brackets, confirming the robustness of our results. A significant difference in DCBC across parcellations was found by a repeated measures ANOVA with the 13 parcellations as the within-subject factor, $F(12,396) = 100.92$, $p<.001$). Post-hoc paired t-test showed a better cluster validity of Tu (326) against other parcellations (Cohen's $d > 1.2$, Supplementary Figure 9B) in the infant/toddlers at 8-30 months.

To further validate the cluster validity of the parcellations in younger infants, we calculated the DCBC on individuals from all five BCP groups (Supplementary Figure 10). We ran a repeated measures ANOVA with the 12 parcellations as the within-subject factor and the 5 age bins as the between-subject factor on the 13x177 DCBC matrix. There was a significant difference in DCBC across parcellations, $F(12,2064) = 551.31$, $p<.001$), and no interaction between the five age bins and parcellations, $F(48,2064) = 0.76$, $p = 0.88$). Post-hoc paired t-test also showed a better cluster validity (Cohen's $d > 1.2$) of Tu (326) against other parcellations for younger infant groups.

Similar results were observed when calculating a homogeneity Z-score at the group-average level (Supplementary Figure 11-12). Details are provided in Supplementary Materials.

Age-specific Infant Parcellations Have Comparable Cluster Validity to the 2-year-old Parcellation

We generated parcellations using the BCP dataset for five smaller age bins with a 65% merging threshold (Figure 4A). Age-specific infant parcellations were similar to one another (ranging from 352 to 380 parcels, ARI = 0.5-0.6). We calculated DCBC of the age-specific parcellations, the Tu (326) and the Gordon (333) on additional sessions of BCP data from a different set of subjects. A significant difference across parcellations was found with the repeated measures ANOVA with the 3 parcellations as the within-subject factor for 10 months ($F(2,18) = 15.86$, $p<.001$), 12 months ($F(2,20) = 21.52$, $p<.001$), 16 months ($F(2,24) = 21.74$, $p<.001$), 19 months ($F(2,36) = 49.01$, $p<.001$), and 25 months ($F(2,38) = 48.61$, $p<.001$). Using a post-hoc two-tailed paired t-test, we found that the age-specific parcellation outperformed Tu (326) parcellation only at 10 months (FDR-corrected $p = 0.038$) (Figure 4B), and was significantly worse than the Tu (326) parcellation at 19 months (FDR-corrected $p = 0.0065$). Given that the Tu (326) parcellation was derived from a separate dataset from the age-specific parcellations, the current results supported the generalizability and the utility of our Tu (326) parcellation to the age range of 1-2 years.

Since the Wang infant/toddler parcellation (Wang *et al.*, 2023) also had age-specific versions with parcellations from 3,6,9,12,18, and 24 months, we tested whether the age-specific parcellations would best fit the individual FC in a similar age bracket. We found no clear evidence that data from a similar age range was best fit by the age-specific parcellation and that all age-specific Wang parcellations had low DCBC (<0.02) (Supplementary Figure 13).

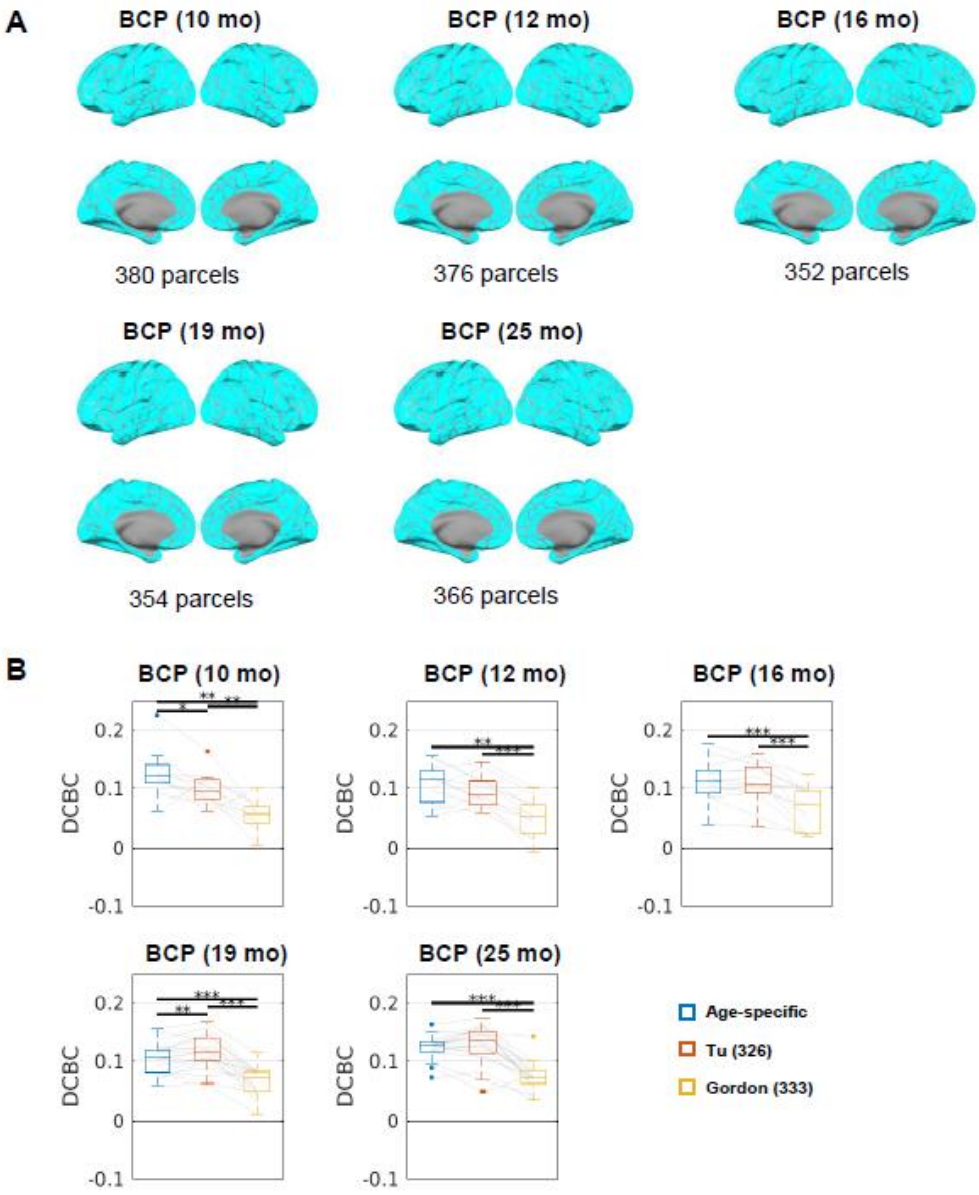

Figure 4. *Age-specific infant area parcellations.* DCBC on a secondary validation dataset of held-out BCP participants using i) the age-specific parcellations, ii) Tu (326), and iii) Gordon (333). ** p<.01, *** p<.001. FDR-corrected for 3 paired t-tests.

Adult Parcellations Based on Functional Connectivity Have a Higher Cluster Validity at Age 6 and Beyond

We determined the fit of area parcellations across the lifespan by testing our set of parcellations across FC in individual neonates (eLABE (Birth)), 3-year-olds (eLABE (Y3)), children (HBN), and young adults (HCP-YA). Neonate FC data were best fit by Myers-Labonte (283) parcellation (Figure 5A), 3-year-old FC data were best fit by the Tu (326) parcellation (Figure 5B). Children (Figure 5C-E, Supplementary Figure 14) and young adult (Figure 5F) FC data were best fit by the Gordon (333) parcellation. Adult and infant parcellations derived from FC rather than anatomy alone have a positive DCBC across all datasets at age 6 and beyond, with the difference in cluster validity across pairs of parcellations demonstrated in Supplementary Figure 15.

The Myers-Labonte parcellation (Myers *et al.*, 2024) included an alternative version that covered most of the brain (height threshold = 90%). Both versions of the

Myers-Labonte parcellation significantly better fit the eLABE data at the birth time point. They were both worse than the Tu (326) parcels at the Y2/Y3 time points, and they had comparable (Myers-Labonte (283), FDR-corrected p≥.05) or worse (Myers-Labonte (370), FDR-corrected p<.05) fit than the Gordon (333) parcels at the Y2/Y3 time points (Supplementary Figure 16).

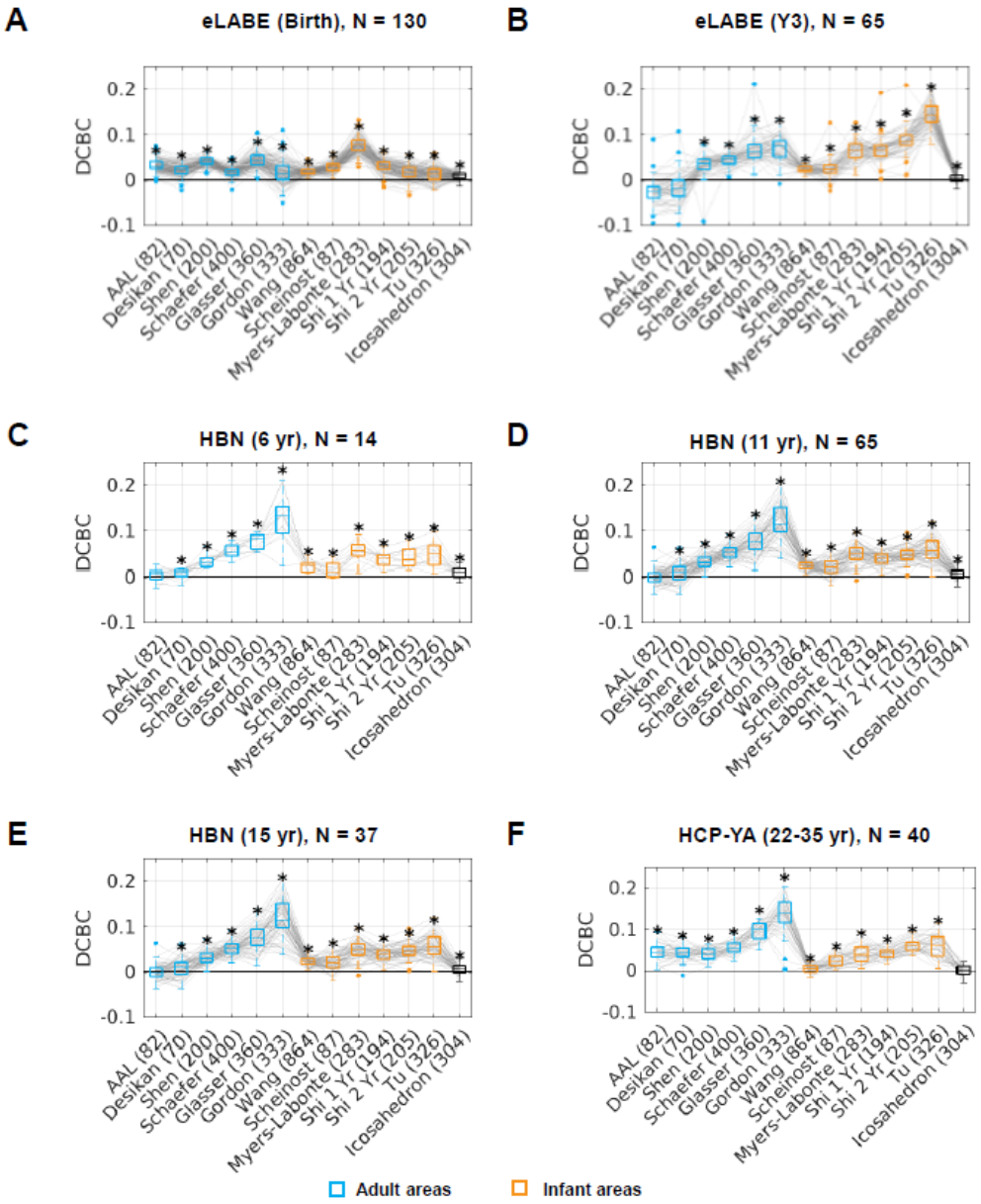

Figure 5. *Cluster validity for different adult and infant parcellations across other developmental stages.* A) a neonate dataset eLABE (Birth), B) an older toddler dataset eLABE (Y3), C-E) a children dataset HBN, and D) a young adult dataset HCP. * p<.05 after FDR-correction

Practical Implications of Using Infant versus Adult Parcellations

To capture the practical implications of using infant versus adult parcellations, we tested the prediction of chronological age from the parcellated connectome and the test-retest reliability of the connectome using the validation dataset (BCP). We observed that the prediction accuracy increased with the number of parcels but

plateaued at around 300 parcels (Supplementary Figure 17A) regardless of adult or infant parcellations.

The spatial distribution of the top 5% of edges with positive and negative correlations was similar across the best-performing infant (Tu (326)) and adult (Gordon (333)) parcellations (Supplementary Figure 17B-C). Medial-visual, motor, and medial parietal areas had the highest number of edges significantly correlated with age while the lateral frontal areas had the lowest number of edges significantly correlated with age (Supplementary 17D-E).

In addition, we computed the test-retest reliability of FC using the Tu (326) and Gordon (333) parcellations on the BCP dataset. We found lower test-retest reliability (as indexed by ICC) in the motor areas and the lateral-medial prefrontal cortex using both parcellations (Supplementary Figure 18).

Community Assignment of Parcels in to Networks

The interactions between the cortical areas form large-scale functional networks or communities (Power *et al.*, 2011; Yeo *et al.*, 2011). We obtained data-driven community assignments using the Tu (326) parcels as the nodes in a graph and optimized for reliable networks that were present across densities (Supplementary Video). Contrary to the fragmented anterior and posterior parts of the default network and fronto-parietal network observed in neonates in the same dataset (Sylvester *et al.*, 2022; Myers *et al.*, 2024), at the age of two the anterior and posterior parts of those networks joined together at higher edge densities (Figure 6A), suggestive of increased long-range FC within the network from 0 to 2 years. We found that at lower edge densities, the default network divides into four local components (posterior default, inferior fronto-parietal, dorsomedial prefrontal cortex (PFC), and ventromedial PFC) instead of distributed components (Andrews-Hanna *et al.*, 2010; Yeo *et al.*, 2011; Gordon *et al.*, 2020), suggestive of more localized FC distribution in 2-year-olds compared to adults. Similarly, the fronto-parietal network can also separated into posterior fronto-parietal, lateral PFC, and anterior PFC at lower edge densities (Figure 6B). The visual network can be separated into primary visual and visual association, similar to adults. The visual association network here has sometimes been described as a component of the dorsal attention network (Yeo *et al.*, 2011; Du *et al.*, 2024). To illustrate the change in long-range FC strengths across neonates, 2-year-olds, and

adults, we visualized the raw connectivity seed maps from different components of the canonical default network (Supplementary Figure 19).

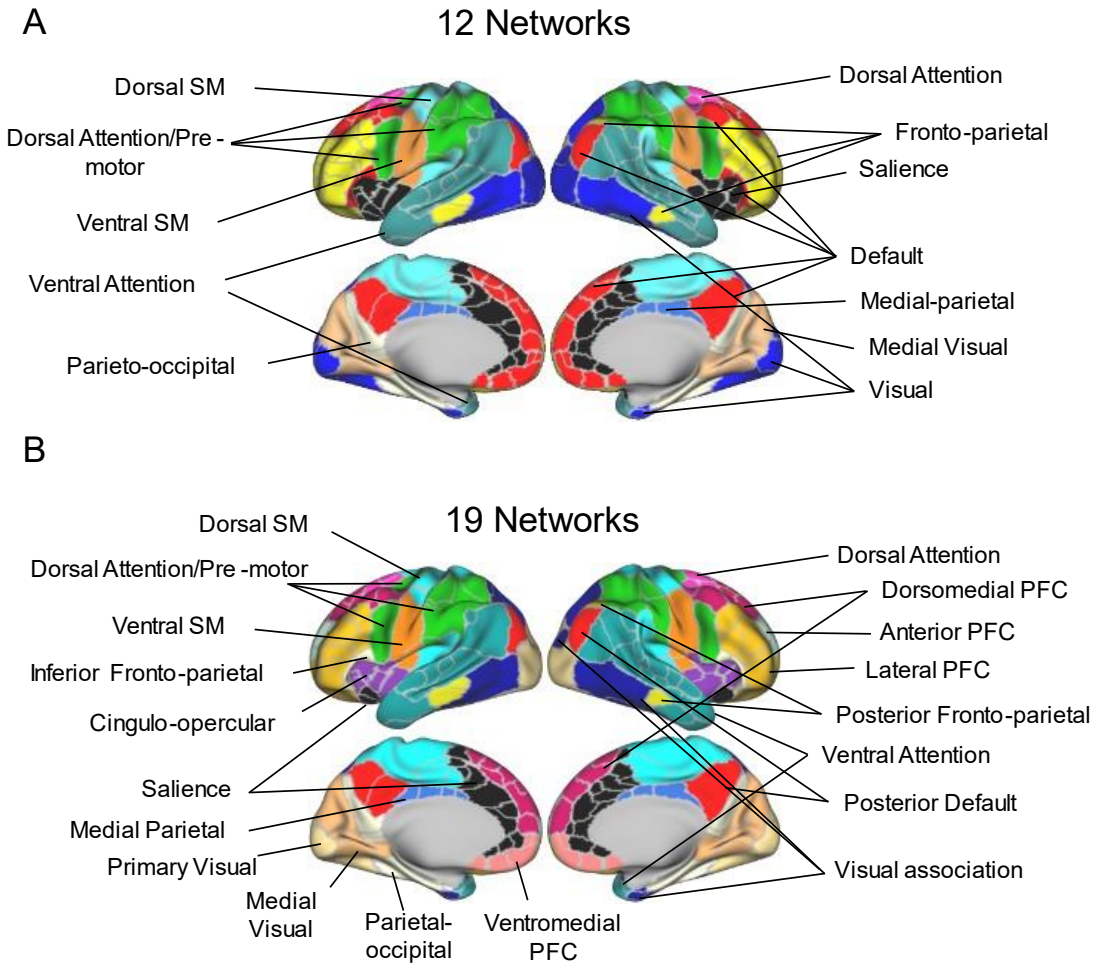

Figure 6. *Assigned community identities for each parcel*. A) Consensus community assignment for 12 networks. B) Finer division of 19 networks. Acronyms: PFC = Prefrontal Cortex, SM = Somatomotor.

Discussion

Boundary Consistency in 2-year-olds is stronger on the Sensorimotor end than on the Association end

We observed that area boundaries on the sensorimotor end of the sensorimotor-association hierarchy tend to be more consistent across subject samples. This observation could be attributed to two factors: 1) interindividual variability was lower in sensorimotor systems (Mueller *et al.*, 2013; Gratton *et al.*, 2018; Kong *et al.*, 2019; Li *et al.*, 2019; Sydnor *et al.*, 2021), or 2) some borders in the sensorimotor systems were sharper, as seen in macaque monkeys (Lewis and Van Essen, 2000).

Area Boundary Maps in 2-year-olds Resembled Adult Area Boundary Maps More than Neonate Area Boundary Maps

Prior literature has described the mechanism of cortical arealization across development as a process that involved the formation of morphogen gradients driven by genetic factors, as well as the activity-dependent refinement of sharp boundaries (Cadwell *et al.*, 2019) influenced by thalamocortical inputs (O'Leary, Chou and Sahara, 2007). Consistent with this view, our current study showed that the putative cortical areas as defined by FC in 2-year-olds were more similar to those in adults than those in neonates. These results suggested that there has been substantial development of area boundaries in early infancy, after which the rate of change slowed down. Another group has found relatively low across-age variability in the boundary maps across 3 months to 24 months, with a multipeak fluctuation in across-age variability (Wang *et al.*, 2023). It might be possible that the most substantial refinement of area boundaries in neonates took place in the first 3 months. Coincidentally, surface area continues to expand dramatically from 29 post-menstrual weeks but decreased in the developmental pace after 3 months (Bethlehem *et al.*, 2022; Huang *et al.*, 2022), further supporting this idea.

Of note, area boundaries from the 2-year-olds did exhibit a higher similarity to those from the neonates than a rotated null model. This observation suggested that there exists some established organization of area boundaries from birth, consistent with the proposed intrinsic proto-mapping of cortical area organizations driven by morphogens in embryonic development (O'Leary, Chou and Sahara, 2007; Tau and Peterson, 2010; Smyser, Snyder and Neil, 2011; Cadwell *et al.*, 2019).

A Coarse-grained Area Parcellation was Optimized for Biological Validity and Utility

Our level of resolution at 326 parcels is comparable to most other adult and infant parcellations. In addition, it is close to the prior estimation of 300-400 cortical areas in humans (Van Essen *et al.*, 2012). Since the resolution has non-negligible effect on measurements such as global graph metrics (Zalesky *et al.*, 2010; Arslan *et al.*, 2018), we believe that keeping the number of parcels similar with popular adult parcellations makes comparison across infants and adults more fair. While another fine-grained infant parcellation exists (Wang *et al.*, 2023), our results suggested that its generalizability to alternative processing or datasets is low as demonstrated by our results. Furthermore, multiple lines of evidence including our analyses suggested that the prediction of demographic and behavioral variables in adults and infants plateau with ~300 parcels (Arslan *et al.*, 2018; Kong *et al.*, 2023) and that a clear correspondence between the FC gradients and the Mesulam hierarchy can be seen regardless of parcellation scheme with more than 300 nodes (Vos de Wael *et al.*, 2020). Therefore, having a fine-grained area parcellation may not necessarily provide a practical advantage in analyses such as examining graph properties of the brain network or multivariate age prediction.

On the other hand, we recognize that different levels of resolution may be useful in different applications (Zalesky *et al.*, 2010; Schaefer *et al.*, 2018). Therefore, we also released the parcellation at multiple resolutions with the caveat that our estimates of the higher-resolution area parcellations might not be as generalizable across individuals and datasets and should be used with caution.

Cluster Validity of Adult Area Parcellations in Developmental Cohorts

We found that while the best-performing adult area parcellation (Gordon (333)) had a worse fit to the functional connectivity data in 0-3 year-olds than the best-performing infant area parcellations, they still beat the random chance and suggested

some resemblance to adult area parcellation in neonates to 3-year-olds. For additional discussion regarding results in prior literature see Supplementary Materials.

Using Adult instead of Infant Area Parcellations Lead to Qualitatively Similar Conclusions for Age Prediction and Test-retest Reliability

We found that prediction accuracy of age increased with parcel number and plateaued around 300 parcels with no clear advantage of the shape and distribution of parcels, consistent with prior literature (Arslan *et al.*, 2018; Kong *et al.*, 2021). Another study found a marginal effect of atlas choice on the prediction of individual psychological and clinical traits and supported the use of data-driven than pre-defined parcellations (Dadi et al. 2019). However, this observation could potentially be attributed to the difference in the number of areas between the data-driven and pre-defined parcellations.

The spatial distribution of test-retest reliability of FC in the infant data was similar to that in adults (Tozzi *et al.*, 2020), albeit numerically lower. This lower reliability could potentially be explained by a combination of the low amount of data (5 min) used for test and retest, the difference in phase-encoding direction in the test and retest scans, and/or transitions between different stages of the sleep cycle in the infant data compared to awake adult scans (Mitra *et al.*, 2017).

While our limited explorations here added credence to conclusions from previous studies using adult parcellations (Kardan *et al.*, 2022; Nielsen *et al.*, 2022), this did not support the notion that the adult parcels were valid representations of the infant areas.

Network Assignments in 2-year-olds Resembled Networks in Adults

We were able to identify fragmented components of canonical adult functional systems consistent with the prior literature using similar techniques on participants in this age range (Eggebrecht *et al.*, 2017; Kardan *et al.*, 2022; Wang *et al.*, 2023). Nevertheless, when weaker connectivity was included, network assignments in 2-year-olds had similar topography to previously reported adult networks (Power *et al.*, 2011; Yeo *et al.*, 2011; Gordon *et al.*, 2016; Ji *et al.*, 2019). This observation was consistent with prior studies suggested that long-range FC tended to develop later than short-range FC with age (Smyser *et al.*, 2010; Smyser, Snyder and Neil, 2011; Spisák *et al.*, 2014; Smyser and Neil, 2015; Thomason *et al.*, 2015; Sylvester *et al.*, 2022).

Despite the similarities to adult networks, we also found important differences in the network assignments in 2-year-olds. First, the temporal lobe remained largely segregated from the canonical default network unlike in adults. Additionally, the motor hand/foot system incorporated part of the inferior parietal lobule and posterior insula, which might suggest some extra plasticity that contributes to multisensory integration during development. This might be driven by the connectivity between inter-effector regions and control network (Gordon *et al.*, 2023). Furthermore, the salience and cingulo-opercular networks were less differentiated from each other, and the cingulo-opercular network was missing the component commonly observed at the cingulate cortex.

It is important to note that the infomap community detection algorithm tends to find more localized clusters when only examining the strongest FC due to the stronger FC at short-distance, especially in developmental cohorts. We suspect that alternative methods which de-emphasizes the distance dependence of FC (Zamani Esfahlani *et al.*, 2020; Sylvester *et al.*, 2022) may retrieve communities more similar to the large-

scale functional systems identified in adults (Petersen and Sporns, 2015). Instead of making a binary decision about whether the networks "connect" or "separate", we believe that it is more important to note the performance of the algorithm across different edge densities and compare it to the adult network topography. Thus, we provide a 12-network model which largely resembles the definition of functional networks observed in adults, and also a 19-network model with a similar granularity to the functional networks defined in neonates with the same eLABE dataset (Myers *et al.*, 2024) targeted at different uses.

It is worth emphasizing that whether the network clusters we identified with functional connectivity corresponds to "functional systems" with specialized functional roles (Power *et al.*, 2011; Yeo *et al.*, 2011; Wig, 2017) remains an outstanding question. They are likely premature forms of the adult systems (Gao, Alcauter, Elton, *et al.*, 2015; Gao, Alcauter, Smith, *et al.*, 2015).The biological validity of the fragmented components we found will need to be validated with task neuroimaging data in infant/toddlers (Yates, Ellis and Turk-Browne, 2021; Yates *et al.*, 2022) in future research. Researchers who use our network model should be fully aware of this limitation.

Practical Recommendations on Using the Tu (326) and Alternative Parcellations

While theoretically, the development of cortical areas may raise a challenge in finding a consistent parcellation that fits all ages, our results here suggested that our 2-year-old parcellation Tu (326) generalized well to fit the FC patterns in 1-to-3-year-olds. We also recognize that two alternative approaches would also be reasonable depending on the goal and motivation of the studies.

1. *Use a canonical adult parcellation map*. Using the same parcellation map can ensure correspondence across age groups (Oishi, Chang and Huang, 2019). However, this method risks not having the best parcellation for each group and introducing noise in the data. Based on our current results, the use of an adult parcellation might be a reasonable choice with limited practical impact on analyses such as age prediction from parcellated connectome.
2. *Using individualized parcellations or functional embedding to find matching relationships*. Several techniques exist to create individual parcellations based on a group-average parcellation prior (Chong *et al.*, 2017; Li *et al.*, 2017, 2019, 2022; Zhao, Tang and Nie, 2020; Kong *et al.*, 2021; Qiu *et al.*, 2022), or to embed connectivity in a latent space to find correspondence across participants (Haxby *et al.*, 2020; Nenning *et al.*, 2020). Additionally, individualized parcellations can be created with highly-sampled individuals using precision functional imaging methods (Laumann *et al.*, 2015; Gordon *et al.*, 2017).

Limitations and future directions

The datasets used for area boundaries had minor differences in acquisition and processing (Supplementary Table 1), which could potentially impact the appearance of area boundaries. In addition, future studies should also investigate how much of the differences between neonate and their older-age counterparts could be attributed to the challenges in the registration of the neonate's brains due to their tissue properties and anatomical differences from the adult brain. Additionally, when testing the generalizability of parcellations to neonates, 2-year-olds and 3-year-olds, we used data from overlapping subjects from the eLABE longitudinal dataset, which might have provided a slight advantage to the Myers-Labonte (283) and Tu (326) parcellations.

In addition, while our parcellations described cortical area organization in 1-to-3-year-olds, future parcellation atlases would benefit from the additional inclusion of subcortical and cerebellar structures. Moreover, the group atlas can be affected by multiple factors including acquisition, resolution, consistency across participants of functional organization within areas, the consistency of system organization between areas, and the consistency of anatomic organization (Shen *et al.*, 2013). Future research with smaller voxels or a better T2* protocol to include signal to noise ratio may further improve the quality of the group parcellation.

One additional confound is that the infant/toddler data were acquired during natural sleep, which has been shown to weaken long-range connectivity within canonical functional systems (Mitra *et al.*, 2017). It is also known that the sleep architecture changes across developmental stages (Kahn *et al.*, 1996), which may contribute to the reduced consistency of infant FC within and across individuals.

Lastly, some of the area parcellations tested were originally generated in volumetric space. However, all datasets used in testing the cluster validity were in the surface space. For convenience, we transformed the area parcellations in the volumetric space to a standard MNI space when necessary and then to the 32k_fs_LR surface mesh using previously described procedures (Arslan *et al.*, 2018). This transformation was imperfect and could have unintentionally favored surface parcellations over volumetric parcellations.

Conclusion

We developed FC gradient-based area parcellations of the neocortical surface for 2-year-olds to be used in future studies of FC in this age range. We found that area boundaries in 2-year-olds were more similar to those in adults than those in neonates. Despite multiple similar efforts in infant-specific area parcellation, our area parcellations achieved the best cluster validity among all parcellations tested on the 1-to-3-year-olds across two independent datasets. We also found that the best performing adult area parcellations provided a better than chance fit to the FC in 1-3-year-olds infant parcellations. Our results lent credence to conclusions from prior work using an adult parcellation for 1-to-3-year-olds, and supported the hypothesis that the most substantial refinement of cortical areas occured in the first few months of life. Our work not only shed new insights into the neurobiology of cortical arealization in humans but also offered practical guidelines for using cortical parcellation for neuroimaging studies in developmental cohorts.

Data and Code Availability

Baby Connectome Project data are available for download at the NIH Data Repository website: https://nda.nih.gov/edit_collection.html?id=2848. Early Life Adversity, Biological Embedding (eLABE) data are available through request at https://eedp.wustl.edu/research/elabe-study/.

All analyses, unless otherwise stated, were implemented with custom MATLAB scripts in the R2020b release. All visualizations were created with custom MATLAB scripts or Connectome Workbench Version 1.5.0.

The code for the generation and evaluation of parcellations are adapted from the MSCcodebase. All parcellations used in CIFTI format are also available to download here.

Author Contributions

JCT, MDW, and ATE conceptualized the project. EMG, TOL, MM and JL provided methodology support and software. JCT and WL conducted a formal analysis. OK, LAM, EF, TKMD, AL, JKK, CS, DD, XW, and YW curated the data. JTE and CDS were responsible for project administration. MDW, JCT, JTE, DMB, BBW, JLL and CDS were responsible for funding acquisition. JCT and MDW wrote the original draft. Everyone contributed to the review and editing of the final manuscript.

Funding

This work is partially supported by the CCSN fellowship from the McDonnell Center for Systems Neuroscience at Washington University School of Medicine in St. Louis to JCT and from NIH grants including EB029343 to MDW. The Baby Connectome Project was supported by NIMH R01 MH104324 and NIMH U01 MH110274.

Declaration of Competing Interests

The authors declared no competing interests directly related to this manuscript.

Acknowledgment

The authors thank Dr. Dustin Scheinost for providing the Scheinost parcellation in MNI space (Scheinost *et al.*, 2016). The authors thank Drs. Zhengwang Wu, Fan Wang, and Gang Li for providing the various versions of Wang parcellation (Wang *et al.*, 2023) in cifti 32k_fs_LRstandard mesh. The authors thank Drs. Wei Gao and Haitao Chen for their suggestions on converting the Shi parcellation (Shi *et al.*, 2018) from infant template volume space to 32k_fs_LRsurface. The authors thank Drs. Matthew Glasser, Timothy Coalson, Caterina Gratton, Diana Hobbs, Stephanie Doerings, Gagan Wig, Da Zhi, and Richard Betzel, M. Catalina Camacho, Scott Marek for discussions on various analyses and datasets.

During the preparation of this work the author(s) used ChatGPT in order to improve the sentence structure. After using this tool/service, the author(s) reviewed and edited the content as needed and take(s) full responsibility for the content of the publication.

References

Abraham, A. *et al.* (2017) 'Deriving reproducible biomarkers from multi-site resting-state data: An Autism-based example', *NeuroImage*, 147, pp. 736–745. Available at: https://doi.org/10.1016/j.neuroimage.2016.10.045.

Andrews-Hanna, J.R. *et al.* (2010) 'Functional-Anatomic Fractionation of the Brain's Default Network', *Neuron*, 65(4). Available at: https://doi.org/10.1016/j.neuron.2010.02.005.

Arslan, S. *et al.* (2018) 'Human brain mapping: A systematic comparison of parcellation methods for the human cerebral cortex', *NeuroImage*, 170, pp. 5–30. Available at: https://doi.org/10.1016/j.neuroimage.2017.04.014.

Autio, J.A. *et al.* (2020) 'Towards HCP-Style macaque connectomes: 24-Channel 3T multi-array coil, MRI sequences and preprocessing', *NeuroImage*, 215, p. 116800. Available at: https://doi.org/10.1016/j.neuroimage.2020.116800.

842 Bethlehem, R. a. I. *et al.* (2022) 'Brain charts for the human lifespan', *Nature*, 604(7906), pp.
843 525–533. Available at: https://doi.org/10.1038/s41586-022-04554-y.

844 Betzel, R.F. *et al.* (2014) 'Changes in structural and functional connectivity among resting-
845 state networks across the human lifespan', *NeuroImage*, 102, pp. 345–357. Available at:
846 https://doi.org/10.1016/j.neuroimage.2014.07.067.

847 Beucher, S. and Meyer, F. (1992) 'The Morphological Approach to Segmentation: The
848 Watershed Transformation', in *Mathematical Morphology in Image Processing*. CRC Press.

849 Bijsterbosch, J. *et al.* (2020) 'Challenges and future directions for representations of
850 functional brain organization', *Nature Neuroscience*, 23(12), pp. 1484–1495. Available at:
851 https://doi.org/10.1038/s41593-020-00726-z.

852 Cadwell, C.R. *et al.* (2019) 'Development and Arealization of the Cerebral Cortex', *Neuron*,
853 103(6), pp. 980–1004. Available at: https://doi.org/10.1016/j.neuron.2019.07.009.

854 Cao, M. *et al.* (2014) 'Topological organization of the human brain functional connectome
855 across the lifespan', *Developmental Cognitive Neuroscience*, 7, pp. 76–93. Available at:
856 https://doi.org/10.1016/j.dcn.2013.11.004.

857 Casey, B.J. *et al.* (2005) 'Imaging the developing brain: what have we learned about
858 cognitive development?', *Trends in Cognitive Sciences*, 9(3), pp. 104–110. Available at:
859 https://doi.org/10.1016/j.tics.2005.01.011.

860 Catalano, S.M. and Shatz, C.J. (1998) 'Activity-Dependent Cortical Target Selection by
861 Thalamic Axons', *Science*, 281(5376), pp. 559–562. Available at:
862 https://doi.org/10.1126/science.281.5376.559.

863 Chong, M. *et al.* (2017) 'Individual parcellation of resting fMRI with a group functional
864 connectivity prior', *NeuroImage*, 156, pp. 87–100. Available at:
865 https://doi.org/10.1016/j.neuroimage.2017.04.054.

866 Cohen, A.L. *et al.* (2008) 'Defining functional areas in individual human brains using resting
867 functional connectivity MRI', *NeuroImage*, 41(1), pp. 45–57. Available at:
868 https://doi.org/10.1016/j.neuroimage.2008.01.066.

869 Cusack, R., McCuaig, O. and Linke, A.C. (2018) 'Methodological challenges in the
870 comparison of infant fMRI across age groups', *Developmental Cognitive Neuroscience*, 33,
871 pp. 194–205. Available at: https://doi.org/10.1016/j.dcn.2017.11.003.

872 Dadi, K. *et al.* (2019) 'Benchmarking functional connectome-based predictive models for
873 resting-state fMRI', *NeuroImage*, 192, pp. 115–134. Available at:
874 https://doi.org/10.1016/j.neuroimage.2019.02.062.

875 Donahue, C.J. *et al.* (2016) 'Using Diffusion Tractography to Predict Cortical Connection
876 Strength and Distance: A Quantitative Comparison with Tracers in the Monkey', *Journal of*
877 *Neuroscience*, 36(25), pp. 6758–6770. Available at:
878 https://doi.org/10.1523/JNEUROSCI.0493-16.2016.

879 Du, J. *et al.* (2024) 'Organization of the human cerebral cortex estimated within individuals:
880 networks, global topography, and function', *Journal of Neurophysiology*, 131(6), pp. 1014–
881 1082. Available at: https://doi.org/10.1152/jn.00308.2023.

882 Eggebrecht, A.T. *et al.* (2017) 'Joint Attention and Brain Functional Connectivity in Infants
883 and Toddlers', *Cerebral Cortex*, 27(3), pp. 1709–1720. Available at:
884 https://doi.org/10.1093/cercor/bhw403.

885 Farahani, F.V., Karwowski, W. and Lighthall, N.R. (2019) 'Application of Graph Theory for
886 Identifying Connectivity Patterns in Human Brain Networks: A Systematic Review',
887 *Frontiers in Neuroscience*, 13. Available at:
888 https://www.frontiersin.org/article/10.3389/fnins.2019.00585 (Accessed: 20 March 2022).

889 Faskowitz, J., Betzel, R.F. and Sporns, O. (2022) 'Edges in brain networks: Contributions to
890 models of structure and function', *Network Neuroscience*, 6(1), pp. 1–28. Available at:
891 https://doi.org/10.1162/netn_a_00204.

892 Felleman, D.J. and Van Essen, D.C. (1991) 'Distributed Hierarchical Processing in the
893 Primate Cerebral Cortex', *Cerebral Cortex*, 1(1), pp. 1–47. Available at:
894 https://doi.org/10.1093/cercor/1.1.1.

895 Flechsig, P. (1901) 'DEVELOPMENTAL (MYELOGENETIC) LOCALISATION OF THE
896 CEREBRAL CORTEX IN THE HUMAN SUBJECT.', *The Lancet*, 158(4077), pp. 1027–
897 1030. Available at: https://doi.org/10.1016/S0140-6736(01)01429-5.

898 Fukuchi-Shimogori, T. and Grove, E.A. (2001) 'Neocortex Patterning by the Secreted
899 Signaling Molecule FGF8', *Science*, 294(5544), pp. 1071–1074. Available at:
900 https://doi.org/10.1126/science.1064252.

901 Gao, W., Alcauter, S., Smith, J.K., *et al.* (2015) 'Development of human brain cortical
902 network architecture during infancy', *Brain Structure and Function*, 220(2), pp. 1173–1186.
903 Available at: https://doi.org/10.1007/s00429-014-0710-3.

904 Gao, W., Alcauter, S., Elton, A., *et al.* (2015) 'Functional Network Development During the
905 First Year: Relative Sequence and Socioeconomic Correlations', *Cerebral Cortex (New York,
906 N.Y.: 1991)*, 25(9), pp. 2919–2928. Available at: https://doi.org/10.1093/cercor/bhu088.

907 Glasser, M.F. *et al.* (2013) 'The minimal preprocessing pipelines for the Human Connectome
908 Project', *NeuroImage*, 80, pp. 105–124. Available at:
909 https://doi.org/10.1016/j.neuroimage.2013.04.127.

910 Glasser, M.F. *et al.* (2016) 'A multi-modal parcellation of human cerebral cortex', *Nature*,
911 536(7615), pp. 171–178. Available at: https://doi.org/10.1038/nature18933.

912 Gordon, E.M. *et al.* (2016) 'Generation and Evaluation of a Cortical Area Parcellation from
913 Resting-State Correlations', *Cerebral Cortex*, 26(1), pp. 288–303. Available at:
914 https://doi.org/10.1093/cercor/bhu239.

915 Gordon, E.M. *et al.* (2017) 'Precision Functional Mapping of Individual Human Brains',
916 *Neuron*, 95(4). Available at: https://doi.org/10.1016/j.neuron.2017.07.011.

Gordon, E.M. *et al.* (2020) 'Default-mode network streams for coupling to language and control systems', *Proceedings of the National Academy of Sciences of the United States of America*, 117(29), pp. 17308–17319. Available at: https://doi.org/10.1073/pnas.2005238117.

Gordon, E.M. *et al.* (2023) 'A somato-cognitive action network alternates with effector regions in motor cortex', *Nature*, 617(7960). Available at: https://doi.org/10.1038/s41586-023-05964-2.

Gratton, C. *et al.* (2018) 'Functional Brain Networks Are Dominated by Stable Group and Individual Factors, Not Cognitive or Daily Variation', *Neuron*, 98(2), pp. 439-452.e5. Available at: https://doi.org/10.1016/j.neuron.2018.03.035.

Grayson, D.S. and Fair, D.A. (2017) 'Development of large-scale functional networks from birth to adulthood: A guide to the neuroimaging literature', *NeuroImage*, 160, pp. 15–31. Available at: https://doi.org/10.1016/j.neuroimage.2017.01.079.

Haxby, J.V. *et al.* (2020) 'Hyperalignment: Modeling shared information encoded in idiosyncratic cortical topographies', *eLife*. Edited by C.I. Baker and F.P. de Lange, 9, p. e56601. Available at: https://doi.org/10.7554/eLife.56601.

Helwegen, K., Libedinsky, I. and Heuvel, M.P. van den (2023) 'Statistical power in network neuroscience', *Trends in Cognitive Sciences*, 27(3), pp. 282–301. Available at: https://doi.org/10.1016/j.tics.2022.12.011.

Hill, J. *et al.* (2010) 'Similar patterns of cortical expansion during human development and evolution', *Proceedings of the National Academy of Sciences*, 107(29), pp. 13135–13140. Available at: https://doi.org/10.1073/pnas.1001229107.

Huang, Y. *et al.* (2022) 'Mapping developmental regionalization and patterns of cortical surface area from 29 post-menstrual weeks to 2 years of age', *Proceedings of the National Academy of Sciences*, 119(33), p. e2121748119. Available at: https://doi.org/10.1073/pnas.2121748119.

Huttenlocher, D.P., Klanderman, G.A. and Rucklidge, W.J. (1993) 'Comparing images using the Hausdorff distance', *IEEE Transactions on Pattern Analysis and Machine Intelligence*, 15(9), pp. 850–863. Available at: https://doi.org/10.1109/34.232073.

Ji, J.L. *et al.* (2019) 'Mapping the human brain's cortical-subcortical functional network organization', *NeuroImage*, 185, pp. 35–57. Available at: https://doi.org/10.1016/j.neuroimage.2018.10.006.

Kahn, A. *et al.* (1996) 'Normal Sleep Architecture in Infants and Children', *Journal of Clinical Neurophysiology*, 13(3), pp. 184–197.

Kaplan, S. *et al.* (2022) 'Filtering respiratory motion artifact from resting state fMRI data in infant and toddler populations', *NeuroImage*, 247, p. 118838. Available at: https://doi.org/10.1016/j.neuroimage.2021.118838.

Kardan, O. *et al.* (2022) 'Resting-state functional connectivity identifies individuals and predicts age in 8-to-26-month-olds', *Developmental Cognitive Neuroscience*, 56, p. 101123. Available at: https://doi.org/10.1016/j.dcn.2022.101123.

956 Kim, J.-H. *et al.* (2023) 'Toward a more informative representation of the fetal–neonatal
957 brain connectome using variational autoencoder', *eLife*. Edited by J. Dubois et al., 12, p.
958 e80878. Available at: https://doi.org/10.7554/eLife.80878.

959 Kong, R. *et al.* (2019) 'Spatial Topography of Individual-Specific Cortical Networks Predicts
960 Human Cognition, Personality, and Emotion', *Cerebral Cortex*, 29(6), pp. 2533–2551.
961 Available at: https://doi.org/10.1093/cercor/bhy123.

962 Kong, R. *et al.* (2021) 'Individual-Specific Areal-Level Parcellations Improve Functional
963 Connectivity Prediction of Behavior', *Cerebral Cortex*, 31(10), pp. 4477–4500. Available at:
964 https://doi.org/10.1093/cercor/bhab101.

965 Kong, R. *et al.* (2023) 'Comparison between gradients and parcellations for functional
966 connectivity prediction of behavior', *NeuroImage*, 273, p. 120044. Available at:
967 https://doi.org/10.1016/j.neuroimage.2023.120044.

968 Larivière, S. *et al.* (2020) 'Multiscale Structure–Function Gradients in the Neonatal
969 Connectome', *Cerebral Cortex*, 30(1), pp. 47–58. Available at:
970 https://doi.org/10.1093/cercor/bhz069.

971 Laumann, T.O. *et al.* (2015) 'Functional System and Areal Organization of a Highly Sampled
972 Individual Human Brain', *Neuron*, 87(3), pp. 657–670. Available at:
973 https://doi.org/10.1016/j.neuron.2015.06.037.

974 Levitt, P. (2003) 'Structural and functional maturation of the developing primate brain', *The
975 Journal of Pediatrics*, 143(4, Supplement), pp. 35–45. Available at:
976 https://doi.org/10.1067/S0022-3476(03)00400-1.

977 Lewis, J.W. and Van Essen, D.C. (2000) 'Mapping of architectonic subdivisions in the
978 macaque monkey, with emphasis on parieto-occipital cortex', *Journal of Comparative
979 Neurology*, 428(1), pp. 79–111. Available at: https://doi.org/10.1002/1096-
980 9861(20001204)428:1<79::AID-CNE7>3.0.CO;2-Q.

981 Li, G. *et al.* (2017) 'Developmental Patterns Based Individualized Parcellation of Infant
982 Cortical Surface', *Medical image computing and computer-assisted intervention : MICCAI ...
983 International Conference on Medical Image Computing and Computer-Assisted Intervention*,
984 10433, pp. 66–74. Available at: https://doi.org/10.1007/978-3-319-66182-7_8.

985 Li, J. *et al.* (2024) 'Network-level enrichment provides a framework for biological
986 interpretation of machine learning results', *Network Neuroscience*, pp. 1–29. Available at:
987 https://doi.org/10.1162/netn_a_00383.

988 Li, M. *et al.* (2019) 'Performing group-level functional image analyses based on homologous
989 functional regions mapped in individuals', *PLOS Biology*, 17(3), p. e2007032. Available at:
990 https://doi.org/10.1371/journal.pbio.2007032.

991 Li, Q. *et al.* (2024) 'Development of segregation and integration of functional connectomes
992 during the first 1,000 days', *Cell Reports*, 43(5), p. 114168. Available at:
993 https://doi.org/10.1016/j.celrep.2024.114168.

Li, Y. *et al.* (2022) 'Atlas-guided parcellation: Individualized functionally-homogenous parcellation in cerebral cortex', *Computers in Biology and Medicine*, 150, p. 106078. Available at: https://doi.org/10.1016/j.compbiomed.2022.106078.

Luppi, A.I. *et al.* (2024) 'Systematic evaluation of fMRI data-processing pipelines for consistent functional connectomics', *Nature Communications*, 15(1), p. 4745. Available at: https://doi.org/10.1038/s41467-024-48781-5.

Marcus, D. *et al.* (2011) 'Informatics and Data Mining Tools and Strategies for the Human Connectome Project', *Frontiers in Neuroinformatics*, 5. Available at: https://doi.org/10.3389/fninf.2011.00004.

Markello, R.D. and Misic, B. (2021) 'Comparing spatial null models for brain maps', *NeuroImage*, 236, p. 118052. Available at: https://doi.org/10.1016/j.neuroimage.2021.118052.

Mitra, A. *et al.* (2017) 'Resting-state fMRI in sleeping infants more closely resembles adult sleep than adult wakefulness', *PLOS ONE*, 12(11), p. e0188122. Available at: https://doi.org/10.1371/journal.pone.0188122.

Mueller, S. *et al.* (2013) 'Individual Variability in Functional Connectivity Architecture of the Human Brain', *Neuron*, 77(3), pp. 586–595. Available at: https://doi.org/10.1016/j.neuron.2012.12.028.

Müller, D., Soto-Rey, I. and Kramer, F. (2022) 'Towards a guideline for evaluation metrics in medical image segmentation', *BMC Research Notes*, 15(1), p. 210. Available at: https://doi.org/10.1186/s13104-022-06096-y.

Myers, M.J. *et al.* (2024) 'Functional parcellation of the neonatal cortical surface', *Cerebral Cortex*, 34(2), p. bhae047. Available at: https://doi.org/10.1093/cercor/bhae047.

Nenning, K.-H. *et al.* (2020) 'Joint embedding: A scalable alignment to compare individuals in a connectivity space', *NeuroImage*, 222, p. 117232. Available at: https://doi.org/10.1016/j.neuroimage.2020.117232.

Nielsen, A.N. *et al.* (2022) 'Maturation of large-scale brain systems over the first month of life', *Cerebral Cortex*, p. bhac242. Available at: https://doi.org/10.1093/cercor/bhac242.

Oishi, K., Chang, L. and Huang, H. (2019) 'Baby brain atlases', *NeuroImage*, 185, pp. 865–880. Available at: https://doi.org/10.1016/j.neuroimage.2018.04.003.

O'Leary, D.D.M., Chou, S.-J. and Sahara, S. (2007) 'Area Patterning of the Mammalian Cortex', *Neuron*, 56(2), pp. 252–269. Available at: https://doi.org/10.1016/j.neuron.2007.10.010.

Petersen, S.E. *et al.* (2024) 'Principles of cortical areas and their implications for neuroimaging', *Neuron*, 0(0). Available at: https://doi.org/10.1016/j.neuron.2024.05.008.

Petersen, S.E. and Sporns, O. (2015) 'Brain Networks and Cognitive Architectures', *Neuron*, 88(1), pp. 207–219. Available at: https://doi.org/10.1016/j.neuron.2015.09.027.

1031 Power, J.D. *et al.* (2011) 'Functional Network Organization of the Human Brain', *Neuron*,
1032 72(4), pp. 665–678. Available at: https://doi.org/10.1016/j.neuron.2011.09.006.

1033 Power, J.D. *et al.* (2012) 'Spurious but systematic correlations in functional connectivity
1034 MRI networks arise from subject motion', *NeuroImage*, 59(3), pp. 2142–2154. Available at:
1035 https://doi.org/10.1016/j.neuroimage.2011.10.018.

1036 Power, J.D. *et al.* (2014) 'Methods to detect, characterize, and remove motion artifact in
1037 resting state fMRI', *NeuroImage*, 84, pp. 320–341. Available at:
1038 https://doi.org/10.1016/j.neuroimage.2013.08.048.

1039 Puxeddu, M.G. *et al.* (2020) 'The modular organization of brain cortical connectivity across
1040 the human lifespan', *NeuroImage*, 218, p. 116974. Available at:
1041 https://doi.org/10.1016/j.neuroimage.2020.116974.

1042 Qiu, W. *et al.* (2022) 'Unrevealing Reliable Cortical Parcellation of Individual Brains Using
1043 Resting-State Functional Magnetic Resonance Imaging and Masked Graph Convolutions',
1044 *Frontiers in Neuroscience*, 16. Available at:
1045 https://www.frontiersin.org/articles/10.3389/fnins.2022.838347 (Accessed: 7 February 2023).

1046 Rosvall, M. and Bergstrom, C.T. (2008) 'Maps of random walks on complex networks reveal
1047 community structure', *Proceedings of the National Academy of Sciences*, 105(4), pp. 1118–
1048 1123. Available at: https://doi.org/10.1073/pnas.0706851105.

1049 Schaefer, A. *et al.* (2018) 'Local-Global Parcellation of the Human Cerebral Cortex from
1050 Intrinsic Functional Connectivity MRI', *Cerebral Cortex (New York, NY)*, 28(9), pp. 3095–
1051 3114. Available at: https://doi.org/10.1093/cercor/bhx179.

1052 Scheinost, D. *et al.* (2016) 'Preterm birth alters neonatal, functional rich club organization',
1053 *Brain Structure and Function*, 221(6), pp. 3211–3222. Available at:
1054 https://doi.org/10.1007/s00429-015-1096-6.

1055 Shen, X. *et al.* (2013) 'Groupwise whole-brain parcellation from resting-state fMRI data for
1056 network node identification', *NeuroImage*, 82, pp. 403–415. Available at:
1057 https://doi.org/10.1016/j.neuroimage.2013.05.081.

1058 Shi, F. *et al.* (2018) 'Functional Brain Parcellations of the Infant Brain and the Associated
1059 Developmental Trends', *Cerebral Cortex*, 28(4), pp. 1358–1368. Available at:
1060 https://doi.org/10.1093/cercor/bhx062.

1061 Shrout, P.E. and Fleiss, J.L. (1979) 'Intraclass correlations: Uses in assessing rater
1062 reliability', *Psychological Bulletin*, 86(2), pp. 420–428. Available at:
1063 https://doi.org/10.1037/0033-2909.86.2.420.

1064 Smith, S.M. *et al.* (2011) 'Network modelling methods for FMRI', *NeuroImage*, 54(2), pp.
1065 875–891. Available at: https://doi.org/10.1016/j.neuroimage.2010.08.063.

1066 Smyser, C.D. *et al.* (2010) 'Longitudinal Analysis of Neural Network Development in
1067 Preterm Infants', *Cerebral Cortex*, 20(12), pp. 2852–2862. Available at:
1068 https://doi.org/10.1093/cercor/bhq035.

Smyser, C.D. and Neil, J.J. (2015) 'Use of resting-state functional MRI to study brain development and injury in neonates', *Seminars in Perinatology*, 39(2), pp. 130–140. Available at: https://doi.org/10.1053/j.semperi.2015.01.006.

Smyser, C.D., Snyder, A.Z. and Neil, J.J. (2011) 'Functional connectivity MRI in infants: Exploration of the functional organization of the developing brain', *NeuroImage*, 56(3), pp. 1437–1452. Available at: https://doi.org/10.1016/j.neuroimage.2011.02.073.

Smyser, T.A. *et al.* (2016) 'Cortical Gray and Adjacent White Matter Demonstrate Synchronous Maturation in Very Preterm Infants', *Cerebral Cortex*, 26(8), pp. 3370–3378. Available at: https://doi.org/10.1093/cercor/bhv164.

Spisák, T. *et al.* (2014) 'Voxel-Wise Motion Artifacts in Population-Level Whole-Brain Connectivity Analysis of Resting-State fMRI', *PLOS ONE*, 9(9), p. e104947. Available at: https://doi.org/10.1371/journal.pone.0104947.

Sydnor, V.J. *et al.* (2021) 'Neurodevelopment of the association cortices: Patterns, mechanisms, and implications for psychopathology', *Neuron*, 109(18), pp. 2820–2846. Available at: https://doi.org/10.1016/j.neuron.2021.06.016.

Sylvester, C.M. *et al.* (2022) 'Network-specific selectivity of functional connections in the neonatal brain', *Cerebral Cortex*, p. bhac202. Available at: https://doi.org/10.1093/cercor/bhac202.

Tau, G.Z. and Peterson, B.S. (2010) 'Normal Development of Brain Circuits', *Neuropsychopharmacology*, 35(1), pp. 147–168. Available at: https://doi.org/10.1038/npp.2009.115.

Thomason, M.E. *et al.* (2015) 'Age-related increases in long-range connectivity in fetal functional neural connectivity networks *in utero*', *Developmental Cognitive Neuroscience*, 11, pp. 96–104. Available at: https://doi.org/10.1016/j.dcn.2014.09.001.

Tozzi, L. *et al.* (2020) 'Test-retest reliability of the human functional connectome over consecutive days: identifying highly reliable portions and assessing the impact of methodological choices', *Network Neuroscience*, 4(3), pp. 925–945. Available at: https://doi.org/10.1162/netn_a_00148.

Tzourio-Mazoyer, N. *et al.* (2002) 'Automated Anatomical Labeling of Activations in SPM Using a Macroscopic Anatomical Parcellation of the MNI MRI Single-Subject Brain', *NeuroImage*, 15(1), pp. 273–289. Available at: https://doi.org/10.1006/nimg.2001.0978.

Van Essen, D.C. *et al.* (2012) 'Parcellations and Hemispheric Asymmetries of Human Cerebral Cortex Analyzed on Surface-Based Atlases', *Cerebral Cortex*, 22(10), pp. 2241–2262. Available at: https://doi.org/10.1093/cercor/bhr291.

Vos de Wael, R. *et al.* (2020) 'BrainSpace: a toolbox for the analysis of macroscale gradients in neuroimaging and connectomics datasets', *Communications Biology*, 3(1), pp. 1–10. Available at: https://doi.org/10.1038/s42003-020-0794-7.

Wang, F. *et al.* (2023) 'Fine-grained functional parcellation maps of the infant cerebral cortex', *eLife*, 12, p. e75401. Available at: https://doi.org/10.7554/eLife.75401.

1108 Wig, G.S. (2017) 'Segregated Systems of Human Brain Networks', *Trends in Cognitive*
1109 *Sciences*, 21(12), pp. 981–996. Available at: https://doi.org/10.1016/j.tics.2017.09.006.

1110 Wig, G.S., Laumann, T.O. and Petersen, S.E. (2014) 'An approach for parcellating human
1111 cortical areas using resting-state correlations', *NeuroImage*, 93, pp. 276–291. Available at:
1112 https://doi.org/10.1016/j.neuroimage.2013.07.035.

1113 Yates, T.S. *et al.* (2022) 'Neural event segmentation of continuous experience in human
1114 infants', *Proceedings of the National Academy of Sciences*, 119(43), p. e2200257119.
1115 Available at: https://doi.org/10.1073/pnas.2200257119.

1116 Yates, T.S., Ellis, C.T. and Turk-Browne, N.B. (2021) 'The promise of awake behaving
1117 infant fMRI as a deep measure of cognition', *Current Opinion in Behavioral Sciences*, 40,
1118 pp. 5–11. Available at: https://doi.org/10.1016/j.cobeha.2020.11.007.

1119 Yates, T.S., Ellis, C.T. and Turk-Browne, N.B. (2023) 'Functional networks in the infant
1120 brain during sleep and wake states', *Cerebral Cortex*, p. bhad327. Available at:
1121 https://doi.org/10.1093/cercor/bhad327.

1122 Yeo, B.T.T. *et al.* (2011) 'The organization of the human cerebral cortex estimated by
1123 intrinsic functional connectivity', *Journal of Neurophysiology*, 106(3), pp. 1125–1165.
1124 Available at: https://doi.org/10.1152/jn.00338.2011.

1125 Zalesky, A. *et al.* (2010) 'Whole-brain anatomical networks: Does the choice of nodes
1126 matter?', *NeuroImage*, 50(3), pp. 970–983. Available at:
1127 https://doi.org/10.1016/j.neuroimage.2009.12.027.

1128 Zamani Esfahlani, F. *et al.* (2020) 'Space-independent community and hub structure of
1129 functional brain networks', *NeuroImage*, 211, p. 116612. Available at:
1130 https://doi.org/10.1016/j.neuroimage.2020.116612.

1131 Zhao, J., Tang, C. and Nie, J. (2020) 'Functional Parcellation of Individual Cerebral Cortex
1132 Based on Functional MRI', *Neuroinformatics*, 18(2), pp. 295–306. Available at:
1133 https://doi.org/10.1007/s12021-019-09445-8.

1134 Zhi, D. *et al.* (2022) 'Evaluating brain parcellations using the distance-controlled boundary
1135 coefficient', *Human Brain Mapping*, 43(12), pp. 3706–3720. Available at:
1136 https://doi.org/10.1002/hbm.25878.

1137 Zuo, X.-N. *et al.* (2017) 'Human Connectomics across the Life Span', *Trends in Cognitive*
1138 *Sciences*, 21(1), pp. 32–45. Available at: https://doi.org/10.1016/j.tics.2016.10.005.

1139